LMSC-D686125

LEVEL III

ADA085651

DEVELOPMENT OF ADVANCED ALUMINUM ALLOYS FROM RAPIDLY SOLIDIFIED POWDERS FOR AEROSPACE STRUCTURAL APPLICATIONS

R. E. Lewis et al.
Lockheed Palo Alto Research Laboratory
3251 Hanover Street
Palo Alto, California 94304

March 1980

Interim Technical Report for Period September 1979–February 1980

Approved for public release; distribution unlimited.

Sponsored by
DEFENSE ADVANCED RESEARCH PROJECTS AGENCY
Arlington, Virginia 22209

Monitored by
AIR FORCE MATERIALS LABORATORY
AIR FORCE WRIGHT AERONAUTICAL LABORATORIES
AIR FORCE SYSTEMS COMMAND
Wright Patterson Air Force Base, Ohio 45433

UNCLASSIFIED

SECURITY CLASSIFICATION OF THIS PAGE (When Data Entered)

REPORT DOCUMENTATION PAGE

READ INSTRUCTIONS BEFORE COMPLETING FORM

1. REPORT NUMBER

2. GOVT ACCESSION NO. AD-A085651

3. RECIPIENT'S CATALOG NUMBER (9)

4. TITLE (and Subtitle)

(6) DEVELOPMENT OF ADVANCED ALUMINUM ALLOYS FROM RAPIDLY SOLIDIFIED POWDERS FOR AEROSPACE STRUCTURAL APPLICATIONS.

5. TYPE OF REPORT & PERIOD COVERED

Interim Technical Report, [redacted] 15 Sep 79 - [redacted] 4 Feb 1980

6. PERFORMING ORG. REPORT NUMBER

(14) LMSC-D686125

7. AUTHOR(s)

(10) R. E./Lewis [redacted] I.G./Palmer D.D./Crooks H./Paris F./Billman

8. CONTRACT OR GRANT NUMBER(s)

~~ARPA Order 3417~~

~~Contract~~ F33615-78-C-5203,

(15) ARPA Order-3417

9. PERFORMING ORGANIZATION NAME AND ADDRESS

Lockheed Palo Alto Research Laboratory
Lockheed Missiles & Space Company, Inc.
3251 Hanover Street, Palo Alto, CA 94304

10. PROGRAM ELEMENT, PROJECT, TASK AREA & WORK UNIT NUMBERS

(16) Project 3417

11. CONTROLLING OFFICE NAME AND ADDRESS

Defense Advanced Research Projects Agency (DoD)
1400 Wilson Boulevard
Arlington, VA 22209

12. REPORT DATE

(11) March 1980

13. NUMBER OF PAGES

82

14. MONITORING AGENCY NAME & ADDRESS (if different from Controlling Office)

Air Force Materials Laboratory
Air Force Systems Command
Wright-Patterson Air Force Base, Ohio 45433

15. SECURITY CLASS. (of this report)

UNCLASSIFIED

15a. DECLASSIFICATION/DOWNGRADING SCHEDULE

16. DISTRIBUTION STATEMENT (of this Report)

Approved for public release; distribution unlimited. (12) 85

17. DISTRIBUTION STATEMENT (of the abstract entered in Block 20, if different from Report)

18. SUPPLEMENTARY NOTES

Other authors are: I. G. Palmer and D. D. Crooks, LMSC, Inc.; H. Paris and F. Billman, ALCOA; E. A. Starke, Jr., A. Gysler, E. E. Underwood, and R. Crooks, Georgia Institute of Technology.

19. KEY WORDS (Continue on reverse side if necessary and identify by block number)

aerospace structures	Al-Li-Mn	microstructures
rapidly solidified powders	Al-Li-Zr	mechanical properties
aluminum alloy	Al-Fe-Ni-Co	methodology for predicting wt. savings
Al-Li	Al-Mn-Si	Al-Li-Fe-Ni
Al-Cu-Li	alloy development	Al-Li-Fe-Co

20. ABSTRACT (Continue on reverse side if necessary and identify by block number)

Advanced aluminum alloys are being developed that will provide major payoffs in terms of weight savings for new aerospace structures. The two property goals are: (1) a 30-percent increase in modulus of elasticity-to-density ratio, and (2) a 20-percent increase in modulus of elasticity-to-density ratio plus a 20-percent increase in strength-to-density ratio, when compared to Al 7075-T76 and without a significant loss in other properties important for structural applications.

The program is organized into three phases: 1 – a fundamental alloy and process development study; 2 – scale-up of two best alloys and evaluation of mill product forms.

DD FORM 1 JAN 73 1473 EDITION OF 1 NOV 65 IS OBSOLETE

UNCLASSIFIED

SECURITY CLASSIFICATION OF THIS PAGE (When Data Entered)

210118

3 – design evaluation involving selected redesign of aerospace components, analysis of payoffs, and recommendations for manufacturing technology development. Phase 1 activity, to be completed in the first two years, is organized into four Tasks: 1 – development of advanced aluminum alloys containing lithium; 2 – development of advanced aluminum alloys that do not contain lithium; 3 – quantitative microstructural analyses and mechanical property correlations; 4 – study of aerospace structural applications for advanced aluminum alloys including development and application of a method for predicting weight savings. Phase 1 activity is described below; Phases 2 and 3 have not been initiated.

In the development of aluminum alloys containing lithium, argon atomized splat particulate was prepared for the eight first-iteration alloys. The first four contain 3 wt % Li, 2 to 4 wt % Cu, and Zr or Mn as grain refiners, and the second four contain 3 wt % Li and approximately 1 wt % of various dispersiod-forming elements. Extrusions were prepared for each alloy, and longitudinal tensile properties were obtained for underaged, peak-aged and overaged material. Modulus-to-density ratios were all about 30 percent higher than 7075-T76, and strength was close to 7075-T76 typical values for seven of the alloys. Tensile elongation was 2.7 to 6.3 percent.

A number of processing variables are being evaluated for effect on properties. These variables include particulate screening extrusion ratio, extrusion aspect (width-to-thickness) ratio, solution treatment temperature and aging time. Detailed microstructural examination (optical, TEM, SEM) has been performed of selected alloys with various extrusion and heat treatment processes to relate microstructure and properties.

In the development of nonlithium-containing aluminum alloys, a total of 23 lots of air and argon atomized splat particulate and air atomized fine powder was prepared for the eight first-iteration alloys. The first four alloys contain Fe, Ni, and Co, the second four contain Mn or Mn and Si. Suitable cold and hot compaction and extrusion procedures were developed for these nonheat-treatable alloys and extrusions were successfully prepared. Tensile properties were obtained; the best combination of properties were exhibited by Al-3.5Fe-2.5Ni-4.2Co which had a yield strength of 360 MPa and 9% elongation. Effects of particulate type, atmosphere for particulate generation, and thermal processing variables on tensile properties were evaluated.

FOREWORD

This Interim Technical Report was prepared by Lockheed Missiles & Space Company, Inc., Palo Alto, California, under USAF Contract F33615-78-C-5203. The work is sponsored by the Defense Advanced Research Projects (DoD), Arlington, Virginia, under ARPA Order 3417 with Dr. E. C. van Reuth (Materials Sciences Division) as Cognizant Director, and is administered by the Air Force Materials Laboratory, Wright-Patterson Air Force Base, Ohio, with Dr. Lawrence R. Bidwell (AFWL/MLLS) as Program Manager.

This report covers the period 5 September 1979 to 4 February 1980 as part of an ongoing program to develop advanced aluminum alloys from rapidly solidified powders for aerospace structural applications.

Mr. R. E. Lewis of LMSC, is the Principal Investigator on this program. Other principal contributors to this report are as follows:

I. G. Palmer and D. D. Crooks – LMSC
Section 2.1, Development of Alloys Containing Lithium

H. Paris and F. Billman – ALCOA Laboratories
Section 2.2, Development of Nonlithium-Containing Alloys

E. A. Starke, Jr., A. Gysler, E. E. Underwood, and R. Crooks – Georgia Institute of Technology
Section 2.3, Quantitative Microstructural Analysis and Mechanical Property Correlations

SUMMARY

Advanced aluminum alloys are to be developed that will provide major payoffs for important new aircraft, spacecraft, and missile systems in the next decade. Payoffs will result from weight savings of structural components which, in turn, lead to increased range, payload, service life, and decreased life-cycle cost. Recently conducted feasibility and design tradeoff studies provide a basis for selecting certain property goals for improved aluminum alloys that will result in significant weight savings. These property goals are as follows:

- Goal A. Specific Elastic Modulus: 33.1 $MNmkg^{-1}$ (133×10^6 in.*)
- Goal B. Specific Elastic Modulus: 30.4 $MNmkg^{-1}$ (122×10^6 in.*)
  Specific Yield Strength: 198 $kNmkg^{-1}$ (796×10^3 in.*)

OBJECTIVE

The objective of this program is to develop advanced aluminum alloys from rapidly solidified powders that meet specific property goals. In addition, the program is to establish a metallurgical basis suitable for manufacturing scaleup and application to new weapon systems.

SCOPE

The program is divided into three phases, each consisting of a number of tasks. Phase 1 involves fundamental alloy development studies and consolidation process development and optimization. The most promising alloys are to be selected, produced in simple mill form, and evaluated in Phase 2. Phase 3 will be a design evaluation involving selected redesign of aerospace components, analysis of payoffs, and recommendations for manufacturing technology.

---

*Units are actually (lbf/lbm) in.

The effort during the first two years is devoted solely to Phase 1.

TECHNICAL PROCESS

Summary of activity to date for this program follows:

- TASK 1. Development of Aluminum Alloys Containing Lithium

  A total of 125 kg (276 lb) of argon atomized splat particulate was prepared for evaluation of the eight first-iteration alloys, designed to meet specific stiffness goals. All contain approximately 3 wt.% Li and either 2 to 4 wt.% Cu or approximately 1 wt.% of various dispersoid-forming elements. Melt compositions along with size distribution and morphology of the splat have been obtained; microstructure of the most promising alloys in splat form has been characterized. Extrusions have been prepared from unsegregated and segregated splat for all eight alloys, and mechanical and physical properties were measured for under-, peak-, and overaged conditions. Metallographic and fractographic studies of these alloys have been conducted to relate microstructure and properties. Variations in extrusion ratio and heat-treatment have been evaluated for their effect on obtaining optimum combinations of tensile strength and ductility while meeting program goals for specific stiffness.

- TASK 2. Development of Nonlithium-Containing Aluminum Alloys

  A total of 1112 kg (2452 lb) of powder and splat particulate was prepared for evaluation of the eight first-iteration alloys designed to meet specific stiffness property goals, and include both air and argon atomized splat and air atomized powder lots. These include Fe-Ni-Co, Mn, or Mn + Si alloying additions. Melt compositions along with screen fraction analysis, morphology and microstructure of the splat and atomized powder have been obtained. Thermal stability of the rapidly solidified alloys was characterized by Guinier analysis and transmission electron microscopy of aged particulate.

The results of this study were used to successfully conduct hot pressing and extrusion thermal cycles. Mechanical properties were measured for 35 alloy-particulate type-processing cycle combinations in the as-extruded condition. Note that these particular alloys are nonheat-treatable.

- TASK 3. Quantitative Microstructural Analysis and Mechanical Property Correlations

An investigation of microstructures, mechanical behavior, and fractographic features was undertaken for two alloys (Al-4Cu-3Li and Al-3Li-1.5Mn) extruded from splat particulate, and selected comparisons made with comparable ingot metallurgy material. Comparisons were made of grain size and shape, crystallographic texture (pole figures), and aging response (hardness versus aging time). Tensile tests were conducted of the Al-Cu-Li and Al-Li-Mn alloys, and microstructures and fractographic features were analyzed for solution treated and under-, peak-, and overaged conditions.

- TASK 4. Application Studies

A comprehensive model for prediction of weight saving in selected aerospace structures by application of advanced aluminum alloys was adapted to a carrier-based naval patrol plane (S-3A) and an advanced tactical fighter (ATF). The effect of secondary structural material property criteria on payoff in terms of weight savings was also evaluated. The minimum acceptable values of damage tolerance assessment (DADTA) properties required for compression critical structures were derived for fighter, patrol, and transport aircraft.

IMPORTANT FINDINGS AND CONCLUSIONS

In the Al-3Li-X splat alloy extrusions, the optimum combination of properties was exhibited by Alloy 1.2A (Al-3Li-2Cu-0.2Zr): 413 MPa (60 ksi) yield strength and 6.3% elongation, and in the solution treated and moderately overaged condition. All the alloys meet the Contract Goal A requirement for specific stiffness.

Tensile properties of Al-3Li-X alloy extrusions prepared from a selected splat screen fraction range (-8/+100) were similar to extrusions prepared from unscreened splat. Tensile properties of the same alloys using the selected screened splat and extruded at 20:1 ER were similar to 8:1 ER extrusions, in the solution treated and under-, peak-, and overaged conditions. Tensile fracture often initiated at inclusions possibly associated with nonsplat particulate, indicating that simple screening does not remove enough of the nonsplat particles to significantly improve tensile properties.

Reducing the Cu content from 4.0 to 2.0 wt.% in Al-3Li-Cu splat alloys reduces but does not eliminate the presence of brittle intermetallics of Al-Li-Cu. Elimination of the intermetallic in an Al-3Li-Cu alloy is expected to be achieved by reducing Cu to 1.5 wt.%.

Comparison of tensile strength and ductility data for Al-3Li-X alloys in the present study with published results of other studies indicates extrusion shape has a large effect, and is believed to be due to differences in crystal texture as well as alloy composition. Strong differences in crystal texture in high-strength commercial alloys are known to have a significant effect on tensile properties.

TEM examination of thin foils from deformed tensile samples of the Al-3Li-X splat alloys suggests that slip occurs homogeneously, and no extensive shear band formation was found, as reported for ingot metallurgy alloys of comparable composition.

For the nonlithium-containing alloys, the highest yield strength was exhibited by Alloy 2.4A (Al-4.3Fe-5Ni-5Co): 512 MPa (74 ksi), with 3-percent elongation, and 0.6 NTS/YS ratio. Alloy 2.2A (Al-3.5Fe-2.5Ni-4.2Co) exhibited the best combination of properties: 360 MPa (52 ksi) yield strength, 9-percent elongation, and 1.5 NTS/YS ratio. Alloy 2.6A (Al-9.7Mn-2.5Si) had the next best combination of properties: 312 MPa (45 ksi) yield strength, 14-percent elongation, and 1.6 NTS/YS ratio.

The addition of 2.5 wt.% Si to an Al-9.7 wt.% Mn alloy increased both tensile strength and ductility, suggesting that even higher strengths may be achieved with acceptable ductility by additions of more than 2.5 wt.% Si with the same Mn:Si ratio.

Tensile properties of Al-Fe-Ni-Co and Al-Mn-Si alloys made from splat produced in air were higher than those made from splat produced in argon. Tensile properties of the same alloys were similar for both splat and fine atomized powder product, with the latter exhibiting slightly higher strength and lower ductility. The anisotropy in tensile properties (longitudinal versus transverse) was also similar for splat and fine atomized powder products.

CONTENTS

Section		Page

ILLUSTRATIONS

TABLES

Section 1
INTRODUCTION

1.1 IMPROVED STRUCTURAL MATERIAL NEEDS FOR AEROSPACE SYSTEMS IN THE NEXT DECADE

Three major new aerospace systems, to be developed in the next decade, will have significantly advanced military capabilities. They are an Advanced Tactical Fighter (Air Force), Vertical/Short Takeoff and Landing Reconnaissance Airplane (Navy), and Advanced Fleet Ballistic Missile (Navy). In each of these, structural materials exhibiting selectively improved properties are needed to realize the desired range, payload, and service-life improvements.

To achieve those property goals that will have a maximum payoff in these new systems, design tradeoff and material development studies have been and are being performed. These studies include advanced aluminum alloys, titanium alloys, and composites. Two important considerations in these studies are pertinent to the subject work reported herein:

(1) Improved aluminum alloys are of major interest to aerospace manufacturers because of the extensive existing manufacturing technology and capability directly suitable for this class of alloys.

(2) The development of improved aluminum alloys that exhibit significantly higher stiffness and/or strength properties has been shown to be technically feasible.

The following subsection highlights recently completed and some ongoing design tradeoff studies that provide a basis for selecting property goals for this alloy/process development program.

1.2 PAYOFFS IN SELECTED AEROSPACE SYSTEMS

1.2.1 Advanced Tactical Fighter

As part of an ongoing study* for the U.S. Air Force for air-to-surface technology in 1985, one aerospace manufacturer analyzed a close-coupled canard supersonic fighter-interceptor aircraft. Analysis was made of payoffs resulting from application of advanced stiffness aluminum alloys, advanced aluminum powder metal alloys such as CT-90 and CT-91, textured titanium, graphite-epoxy composites, FP-aluminum composites, low-cost hybrid composites, beta titanium isothermally forged, and low-temperature formable titanium sheet. These advanced materials were included in the study on the assumption that they would be available by 1985, provided that appropriate development and scaleup attention is directed to them.

A high-stiffness aluminum alloy exhibiting a 30-percent increase in modulus-to-density ratio was identified as the best choice for a number of major structural components. Weight saved and related cost figures for these components were estimated, compared with aluminum alloys commercially available in 1975. The weight saved was projected to a life-cycle cost savings of $469,000 per airplane. These savings were attributed to increased life as well as reduced maintenance and inspection.

The life-cycle cost savings result in a projected total savings of $234 million when applied to a fleet of 500 airplanes. Of the advanced materials concepts considered, the highest payoff 1985 technology identified was the high-modulus, low-density advanced aluminum alloy. Although advanced composites were found to offer competitive weight savings for many complex components such as the fuselage section, they were not recommended for development for such applications because of the high fabrication costs involved, estimated to be more than six times higher than for advanced aluminum alloys.

---

*Advanced information was provided by the U.S. Air Force Materials Laboratory, Wright-Patterson AFB, Ohio.

1.2.2 Vertical/Short Takeoff and Landing Airplane

In the preliminary design tradeoff studies of a recently completed contract investigating the feasibility of developing advanced aluminum alloys, the following property goals were considered and weight savings calculated for each of the aluminum alloy major components in the airframe (Ref. 1). One alloy was assumed to have a 20-percent higher modulus and 10-percent lower density, compared to Al 7075-T76, without significant loss in strength, toughness, fatigue behavior, or stress corrosion resistance. The other alloy was assumed to have a 20-percent higher strength and 10-percent lower density, compared to Al 7075-T76, without significant loss in modulus, toughness, fatigue behavior, or stress corrosion resistance.

Selective application of the two advanced aluminum alloys used in the optimum combination would increase payload 44 percent or increase range by 23 percent for a constant takeoff weight airplane. This significant payoff is achieved in a high-performance version of the V/STOL by a 17-percent weight savings in the wing, fuselage, and tail structure. The tradeoff study also indicated that the range of payload improvements is approximately proportional to the percentage improvement of stiffness and strength.

1.2.3 Advanced Fleet Ballistic Missile

In the same feasibility study (Ref. 1), the C-4 Trident FBM forward adaptor shell was analyzed for potential weight savings as applied closely to the D5 Advanced Trident FBM forward adaptor. The critical design criterion for the forward adaptor shell is stiffness. Substitution of a new aluminum alloy exhibiting 33-percent higher *specific stiffness* resulted in an estimated 16-percent saving in weight of the 56-lb

1. R. E. Lewis, D. Webster, and I. G. Palmer, A Feasibility Study for Development of Structural Aluminum Alloys From Rapidly Solidified Powders for Aerospace Structural Applications, Lockheed Palo Alto Research Laboratory Final Report, Air Force Contract F33615-77-C-5186, Technical Report No. AFML-TR-78-102, July 1978.

1.2.2 Vertical/Short Takeoff and Landing Airplane

In the preliminary design tradeoff studies of a recently completed contract investigating the feasibility of developing advanced aluminum alloys, the following property goals were considered and weight savings calculated for each of the aluminum alloy major components in the airframe (Ref. 1). One alloy was assumed to have a 20-percent higher modulus and 10-percent lower density, compared to Al 7075-T76, without significant loss in strength, toughness, fatigue behavior, or stress corrosion resistance. The other alloy was assumed to have a 20-percent higher strength and 10-percent lower density, compared to Al 7075-T76, without significant loss in modulus, toughness, fatigue behavior, or stress corrosion resistance.

Selective application of the two advanced aluminum alloys used in the optimum combination would increase payload 44 percent or increase range by 23 percent for a constant takeoff weight airplane. This significant payoff is achieved in a high-performance version of the V/STOL by a 17-percent weight savings in the wing, fuselage, and tail structure. The tradeoff study also indicated that the range of payload improvements is approximately proportional to the percentage improvement of stiffness and strength.

1.2.3 Advanced Fleet Ballistic Missile

In the same feasibility study (Ref. 1), the C-4 Trident FBM forward adaptor shell was analyzed for potential weight savings as applied closely to the D5 Advanced Trident FBM forward adaptor. The critical design criterion for the forward adaptor shell is stiffness. Substitution of a new aluminum alloy exhibiting 33-percent higher specific stiffness resulted in an estimated 16-percent saving in weight of the 56-lb

---

1. R. E. Lewis, D. Webster, and I. G. Palmer, A Feasibility Study for Development of Structural Aluminum Alloys From Rapidly Solidified Powders for Aerospace Structural Applications, Lockheed Palo Alto Research Laboratory Final Report, Air Force Contract F33615-77-C-5186, Technical Report No. AFML-TR-78-102, July 1978.

component. Relative significance of weight saved in this portion of the missile is five times the baseline first-stage motor and interstage. Consequently, the 9 lb saved in the component is equivalent to 45 lb saved in the first-stage motor. This saving contributes a significant (classified) addition to range of the missile and is equivalent to about a 15-lb increase in payload. Significant additional weight savings can be expected in other portions of the adaptor section and in the equipment section by application of a high specific stiffness alloy.

1.3 PLAN FOR ALLOY DEVELOPMENT

Based on the above design tradeoff studies and other considerations, a program was formulated to develop advanced aluminum alloys from rapidly quenched particulate. The objective and scope are described in the following paragraphs.

1.3.1 Objective

The objective of this program is to develop advanced aluminum alloys that meet specific property goals. In addition, the program is to establish a metallurgical basis suitable for manufacturing scaleup and application to new weapon systems. Goal A is a 30-percent increase in specific modulus of elasticity relative to Al 7075-T76, without significant loss in strength, toughness, fatigue strength, or stress-corrosion resistance. Goal B is a 20-percent increase in specific modulus of elasticity accompanied by a 20-percent increase in specific strength, without significant loss in toughness, fatigue strength, or stress-corrosion resistance. The resulting property goals are as follows:

- Goal A. Specific elastic modulus: 33.1 $MNmkg^{-1}$ (133×10^6 in.*)
- Goal B. Specific elastic modulus: 30.4 $MNmkg^{-1}$ (122×10^6 in.*)
  Specific yield strength: 1.98 $kNmkg^{-1}$ (796×10^3 in.*)

*Units are actually (lbf/lbm) in.

1.3.2 Scope

The program is divided into three phases, each consisting of a number of tasks. Phase 1 involves fundamental alloy development studies and consolidation process development and optimization. The most promising alloys are to be selected, produced in simple mill form, and evaluated in Phase 2. Phase 3 will consist of a design evaluation using the properties of the alloys evaluated in Phase 2.

This program was initiated in September 1978 and is scheduled for completion in 3-1/2 years. The effort during the first 2 years will be devoted to Phase 1 only. This report describes activity in the reporting period for each of the four tasks comprising Phase 1.

Section 2
EXPERIMENTAL PROCEDURES AND RESULTS

This section describes activities conducted in the reporting period on Phase 1, Alloy Development. Activity on Phases 2 and 3 will not be initiated until Phase 1 is completed.

2.1 TASK 1 – DEVELOPMENT OF ALLOYS CONTAINING LITHIUM

This task is being conducted by the Lockheed Palo Alto Research Laboratories. The first iteration of eight alloys containing 3 wt. % Li to meet program goal A of 30-percent increase in specific modulus were previously prepared from splat particulate supplied by ALCOA. The processing and microstructure-property studies initiated previously were continued in the present reporting period as follows.

2.1.1 Characterization of Starting Materials

The last remaining ingot of the "commercially pure" lithium used to make splat of alloy 1.3 (Al-4Cu-3Li-0.2Zr) was returned by ALCOA to LMSC for sodium analysis. The analysis showed the sodium level to be 100 ppm, significantly lower than the 500 ppm level previously reported by Research Inorganic Chemical Corporation (Table 3 of Ref. 2). This result explains the low sodium levels observed for Alloy 1.3 in both the melt analysis performed by ALCOA (Table 3 of Ref. 3) and the analysis of consolidated material (Table 1).

---

2. R. E. Lewis, Development of Advanced Aluminum Alloys from Rapidly Solidified Powders for Aerospace Structural Applications, Interim Technical Report for Period September 1978 – March 1979, Air Force Contract F33615-78-C-5203, ARPA Order No. 3417, March 1979.

3. R. E. Lewis, Development of Advanced Aluminum Alloys from Rapidly Solidified Powders for Aerospace Structural Applications, Interim Technical Report for Period March 1979 – September 1979, Air Force Contract F33615-78-C-5203, ARPA Order No. 3417, September 1979.

2.1.2 Characterization of As-Extruded Alloys

Chemical analysis by atomic absorption was performed on all eight first iteration alloys and on alloy 1.1X, using extruded material made from unscreened splat particulate. The results are shown in Table 1. The extrusion compositions are in reasonable agreement with the final melt (book mold) compositions reported previously (Table 3 of Ref. 3).

TABLE 1. CHEMICAL COMPOSITION OF AS-EXTRUDED FIRST-ITERATION LITHIUM-CONTAINING ALLOYS (wt. %)

Alloy No.	Nominal Composition	Cu	Fe	Mn	Mg	Zn	Cr	Ni	Co	Li	Na	K
1.1	Al-4Cu-3Li-0.2Zr	3.8	0.03	0.001	0.003	0.003	0.001	0.001	0.01	3.6	0.0009	0.0005
1.1X	Al-4Cu-3Li	3.7	0.03	0.001	0.001	0.003	0.001	0.001	0.2[illegible]*	2.6	0.0005	0.0007
1.2	Al-3Li-2Cu-0.2Zr	2.2	0.02	0.001	0.001	0.003	0.002	0.001	0.01	2.6	0.0005	0.001
1.3	Al-4Cu-3Li-0.2Zr	3.8	0.02	0.001	0.001	0.002	0.001	0.001	0.04	3.2	0.0006	0.003
1.4	Al-4Cu-3Li-0.4Mn	3.7	0.02	0.001	0.001	0.002	0.001	0.001	0.02	3.3*	0.0006	0.0005
1.5	Al-3Li-1Zr (run no. 2)	0.004	0.67	0.002	0.002	0.02	0.001	0.004	0.01	2.5*	0.002	0.0005
1.6	Al-3Li-1.5Mn	0.06	0.03	1.4	0.001	0.003	0.001	0.001	0.01	3.5*	0.0005	0.0005
1.7	Al-3Li-0.5Fe-0.5Ni	0.005	0.43	0.003	0.001	0.003	0.001	0.53	0.02	3.4	0.0005	0.0005
1.8	Al-3Li-0.5Fe-0.5Co	0.003	0.67	0.002	0.002	0.002	0.002	0.006	0.01	3.4*	0.0005	0.0005

*Average of two analyses; all others are results of single analysis.

2.1.3 Consolidation and Processing

Initial consolidations were made using as-received unscreened particulate. Microstructure and mechanical property results on these materials were described in the second Interim Technical Report. In all subsequent work the particulate of all the first iteration alloys has been screened in order to remove most of the nonsplat particles. The coarse material (+8 screen fraction) and fine material (-100 screen fractions) have been rejected, for all the alloys, based on optical examination of individual screen fractions. In two of the alloys (1.3 and 1.1X) the -50/+100 screen

fraction was also rejected, as it contained a greater amount of nonsplat than the other alloys. Hot pressings have been made from the screened particulate of all the first iteration alloys, including alloy 1.1X. A slightly higher hot pressing temperature, 811 K (1000° F), was used than in the earlier consolidations which used 783 K (950° F). This higher temperature was selected to be the same as the solution heat treatment temperature. All hot pressings were extruded at 700 K (800° F) and at extrusion ratios of 8:1 as used previously, or 20:1.

2.1.4 Characterization of Heat-Treated Alloys

Material Extruded at 8:1 Extrusion Ratio

Rectangular extrusions having a width-to-thickness aspect ratio of 2:1 were made from screened particulate of the two most promising alloys, 1.2 (Al-3Li-2Cu-0.2Zr) and 1.7 (Al-3Li-0.5Fe-0.5Ni) using the 8:1 extrusion ratio. Alloys were solution-treated at 811 K (1000° F) for 0.5 h, water-quenched and aged at 473 K (392° F) for 0.75, 8, and 100 h representing underaged, peak-aged, and overaged conditions.

Tensile Properties. Tensile specimens were tested at room temperature and the results are shown in Table 2. No improvement in elongation values for the peak aged condition was observed in these specimens, as compared to the previous data. The yield strength values were found to be slightly lower than in the previously tested material, probably as a result of the slightly higher aging temperature used [473 K (392° F) as compared to 464 K (375° F) used previously].

Only small increases in elongation values were observed in the underaged and overaged conditions, as compared to the peak aged condition, for both alloys. Significant amounts of delamination were observed on the fracture surfaces, even in the specimens which failed by macroscopic shear. The delaminations corresponded to failure along prior particle boundaries. Failure along these prior particle boundaries may be the main cause of the relatively low elongation values observed and the relatively small improvements in ductility in the underaged and overaged conditions.

TABLE 2. TENSILE PROPERTIES OF CONSOLIDATED SCREENED Al-Li ALLOY PARTICULATE EXTRUDED AT 8:1 RATIO, SOLUTION-TREATED AT 811 K (1000° F) AND AGED AS INDICATED

Alloy No.	Nominal Composition	Extrusion No.	Aging Time at 473 K (392° F) (h)	0.2% Yield Strength (MPa)	(ksi)	Tensile Strength (MPa)	(ksi)	Elongation %
1.2	Al-3Li-2Cu-0.2Zr	1.2A.1	0.75	413	61	491	71	4.7
			8	426	62	491	71	4.3
			100	285	41	373	54	5.2
1.7	Al-3Li-0.5Fe-0.5Ni	1.7A.1	0.75	274	40	355	52	3.8
			8	370*	54	437*	63*	2.9*
			100	240	35	338	49	3.7

* Single specimen result; all others are average values of two tests

Microstructural Observations. TEM studies were performed on the extruded material of alloy 1.7 (Al-3Li-0.5Fe-0.5Ni), in order to characterize the dispersoid particle and oxide particle distributions. The solution heat-treated condition was used, so that no precipitate particles would be visible. Fine dispersoid particles were observed, in the size range 0.05 to 0.5 μm (Fig. 1). The fine grain size (2-5 μm) can also be seen. Oxide particles were mostly found in bands corresponding to prior particle boundaries. Selected area diffraction patterns taken from the oxide particles indicate that the oxide is $LiAlO_2$ which exists in several polymorphic forms. The calculated d spacings agree most closely with the published values for the high pressure form of this oxide. Small amounts of porosity were also observed associated with the oxide particles (Fig. 2). This porosity may be partly responsible for the observed tensile failures along prior particle boundaries.

Material Extruded at 20:1 Extrusion Ratio

Rectangular extrusions having a width-to-thickness ratio of 2:1 were made from screened particulate of alloys 1.2, 1.6, 1.7, and 1.8 and extruded at 20:1 extrusion ratio. The alloys were heat treated at 811 K (1000° F) for 0.5 h, water quenched and aged at 464 K (375° F) for 0.75, 8 or 40 h, representing underaged, peak aged and overaged

L575 2 μm

Figure 1. TEM of Alloy 1.7 (Al-3Li-0.5Fe-0.5Ni), solution-treated 811 K (0.5 h) and water-quenched, showing size and distribution of dispersoid particles.

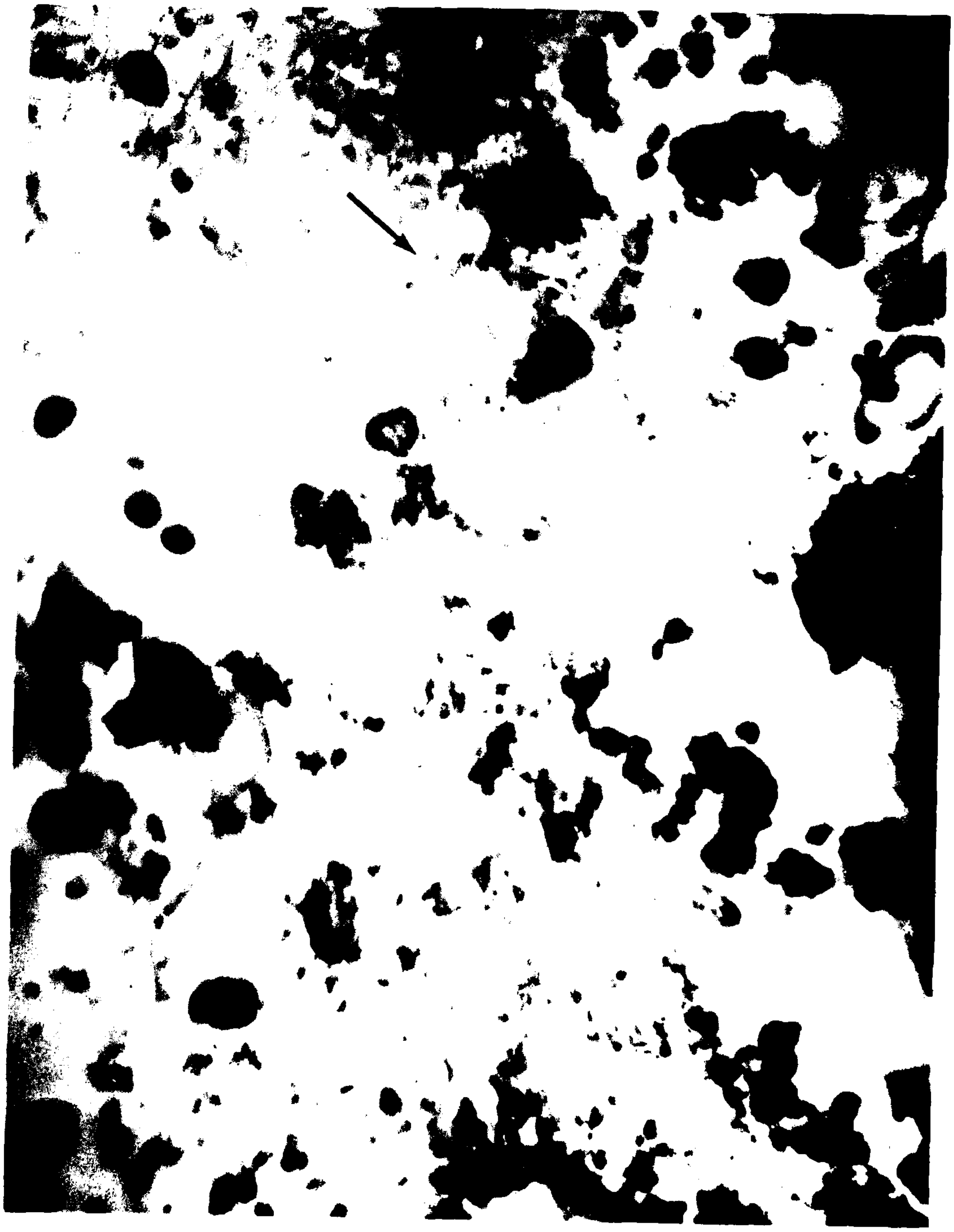

L569

1 μm

Figure 2. TEM of Alloy 1.7 (Al-3Li-0.5Fe-0.5Ni), solution-treated 811 K (0.5 h) and water-quenched, showing bands of oxide particles and small amounts of associated porosity (arrows).

conditions. The 40-h aging time was selected to give an overaged yield strength value closer to that of the underaged condition. The 100-h treatment used previously had given much lower yield strengths (Table 2) and therefore appeared to be an excessively overaged condition.

Tensile Properties. Tensile specimens were tested at room temperature and the results are shown in Table 3. The results are also plotted in Fig. 3 for the peak aged condition and in Fig. 4 for all three aging conditions. A preliminary study of the effect of surface condition on the tensile elongation was made by chemically polishing the surface of selected specimens; they showed a small ductility improvement compared to similar

TABLE 3. TENSILE PROPERTIES OF CONSOLIDATED SCREENED Al-Li ALLOY PARTICULATE EXTRUDED AT 20:1 RATIO, SOLUTION-TREATED AT 811 K (1000° F) AND AGED AS INDICATED

Alloy No.	Nominal Composition	Extrusion No.	Aging Time at 473 K (392° F) (h)	0.2% Yield Strength (MPa)	0.2% Yield Strength (ksi)	Tensile Strength (MPa)	Tensile Strength (ksi)	Elongation (%)	Surface Condition*
1.2	Al-3Li-2Cu-0.2Zr	1.2A-3	0.75	421	61	470	68	2.2	m
			0.75	425	62	491	71	3.5	m
			8	435	63	512	74	3.1	m
			8	456	66	521	76	2.9	m
			40	405	59	489	71	5.2	m
			40	414	60	493	72	6.3	e
1.6	Al-3Li-1.5Mn	1.6A-2	0.75	345	50	396	57	2.4	m
			0.75	355	52	436	63	3.7	m
			8	384	56	456	66	3.0	m
			8	412	60	486	70	3.7	m
			40	376	55	470	68	4.2	m
			40	387	56	476	69	4.3	e
1.7	Al-3Li-0.5Fe-0.5Ni	1.7A-2	0.75	333	48	414	60	4.3	m
			0.75	328	48	336	49	0.9	m
			8	373	54	452	66	4.1	m
			8	382	55	475	69	5.4	m
			40	354	51	425	62	2.9	m
			40	360	52	445	64	5.8	e
1.8	Al-3Li-0.5Fe-0.5Co	1.8A-1	0.75	344	50	399	58	3.1	m
			0.75	348	50	421	61	4.1	m
			8	386	56	457	66	3.9	m
			8	396	57	479	69	5.0	m
			40	355	52	433	63	3.3	m
			40	363	53	443	64	5.4	e

*m mechanically polished; e electrochemically polished

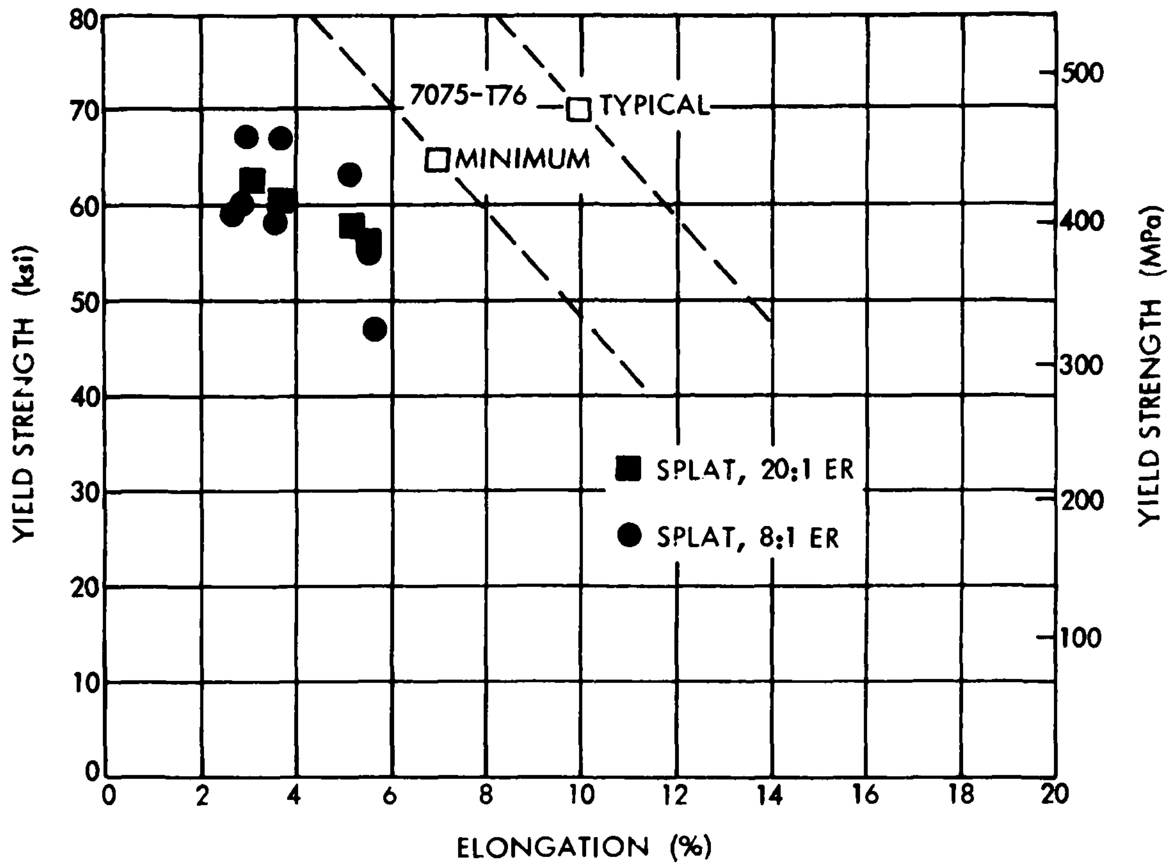

Figure 3. Yield strength versus elongation of Al-3Li-X first-iteration alloys, extruded at 8:1 and 20·1 ratios, peak-aged condition.

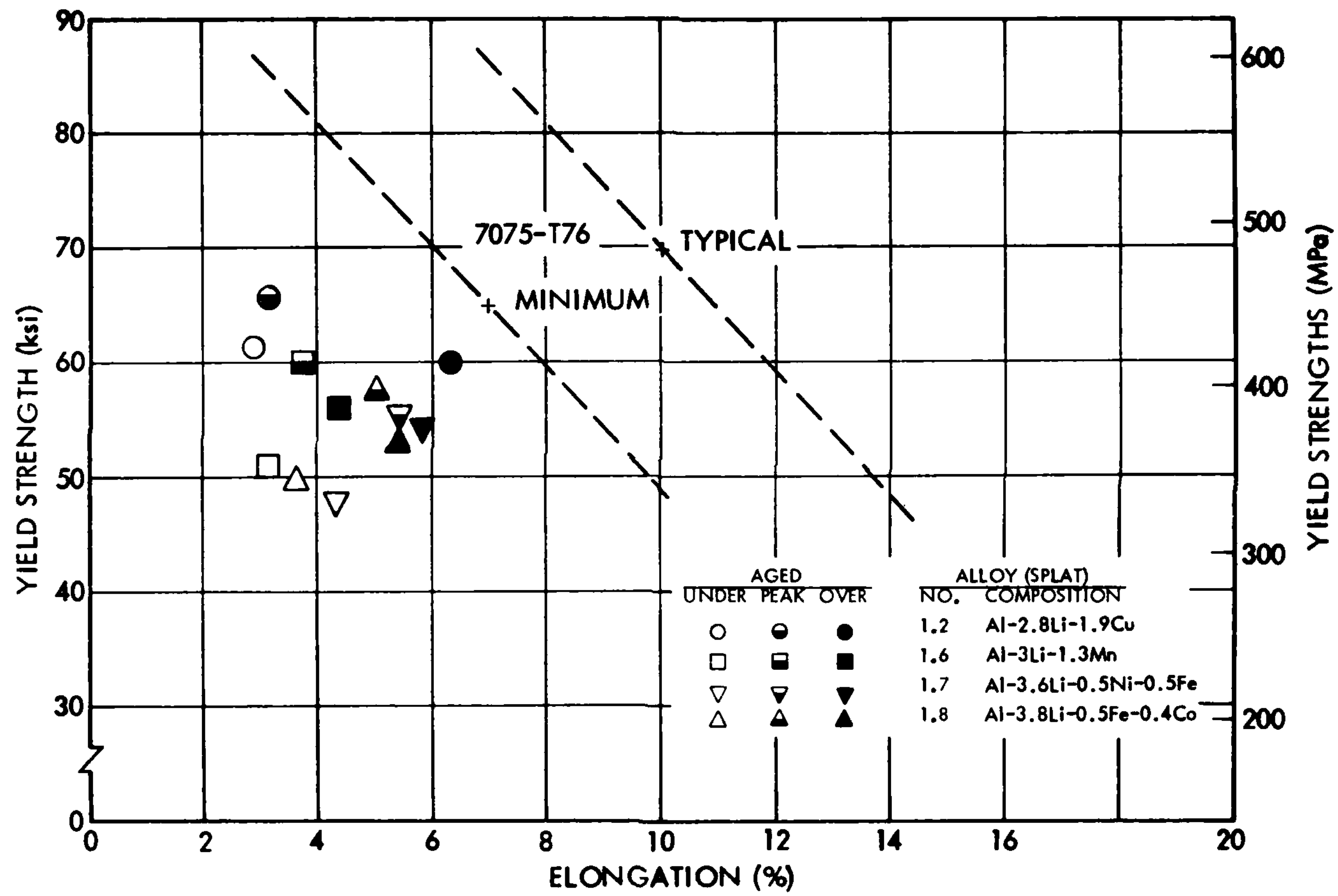

Figure 4. Yield strength versus elongation of Al-3Li-X first-iteration alloys, extruded at 20:1 ratio; underaged, peak-aged, and overaged conditions.

specimens having a mechanically polished surface. The data in Fig. 4 represent the best data obtained. A more systematic study of this effect will be performed in future work.

As shown in Fig. 3, there is no improvement in ductility for the 20:1 ratio extrusions when compared to the results at the lower extrusion ratio. The best combination of properties was shown by Alloy 1.2 in the overaged condition (Fig. 4) with a yield strength of 413 MPa (60 ksi) and an elongation of 6.3%. Significantly less delamination was observed on the fracture surfaces than was observed with the 8:1 extrusion ratio material, but small amounts were still present for all alloys. Most fractures appear to have initiated at the specimen surface, or occasionally at large inclusions. These results suggest that simple screening does not remove enough of the nonsplat particles to significantly improve the tensile properties, and furthermore that increasing the extrusion ratio from 8:1 to 20:1 does not produce a sufficient improvement in the breakup and distribution of oxide particles in prior particle boundaries to further improve tensile ductility.

<u>Microstructural Observations.</u> The microstructure of a fractured tensile specimen of Alloy 1.2 in the peak aged condition was examined. In the underaged and peak-aged conditions, this alloy had shown a number of discontinuities in the stress-strain curve, representing small, incremental extensions of the specimen. None of the other alloys exhibited this behavior. On metallographic examination of Alloy 1.2, some small cracks were found (Fig. 5a) which may relate to the tensile discontinuities; these secondary cracks appear to be the result of interparticle boundary fractures which then arrested. A small volume fraction of intermetallic particles was also observed, significantly less than found in tensile specimens of Alloy 1.1 which contained a higher Cu content (4 wt. %). In Alloy 1.2, particles near the fracture surface were cracked (Fig. 5b), a feature previously observed in Alloy 1.1 (Fig. 17 of Ref. 3); this further demonstrates the brittle nature of the particles. Such particles may contribute to the low ductility in Alloy 1.2, even in the reduced amount present. In subsequent alloy compositions, reducing the amount of Cu to about 1.5 wt. % (close to the solid solubility limit for an alloy containing 3 wt. % Li) will be considered as a method of eliminating this brittle second phase.

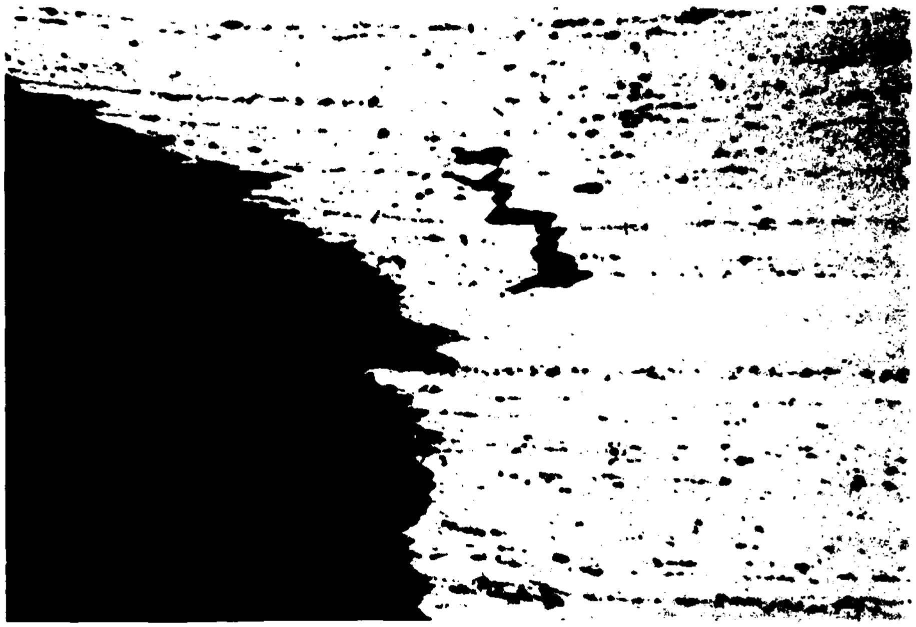

E2739 (a) 40 μm

E2752 (b) 10 μm

Figure 5. Al-3Li-2Cu-0.2Zr consolidated material (20:1 extrusion ratio); solution-treated 811 K, 0.5 h; aged 464 K, 8 h

2.1.5 Discussion

It is instructive to compare the tensile data obtained so far for the best first-iteration alloy (1.2) with the limited published data for Al-Li based alloys of similar Li content. Figure 6 shows yield strength versus elongation data for the peak aged condition of a number of I/M and P/M alloys containing more than 2.5 wt % Li. Comparison with alloys containing lower levels of Li is less pertinent, since they are expected to show superior combinations of strength and ductility but inferior combinations of modulus and density.

The I/M alloy in Fig. 6 showing the best combination of properties (Al-3.5Mg-2.6Li-0.14Zr) was tested in the form of round rod extrusions (Ref. 4), whereas the other I/M alloys were either extrusions of higher aspect ratio (Ref. 5) or alloys tested in sheet form (Ref. 6). Part of the improvement in the properties of the best I/M alloy is probably attributable to texture effects associated with axisymmetric extrusions.

The P/M alloys in Fig. 6 show, in general, better combinations of strength and ductility than the I/M alloys. Only one I/M alloy is superior to P/M Alloy 1.2. The data for the two Al 2024 type P/M alloys containing Li are superior to those of P/M Alloy 1.2 and all the I/M alloys. A wide difference in both strength and ductility is observed between these two alloys for a similar peak aged condition. Examination of the extrusion aspect ratios suggests that texture effects may well account for these differences. Sankaran's material (Ref. 7), showing the highest yield strength, was extruded with a 30:1 extrusion ratio to a round axisymmetric rod. Webster's material (Ref. 8) was extruded with a

---

4. T. H. Sanders, Development of an Al-Mg-Li Alloy, Naval Air Development Center Contract No. N62269-74-C-0438, Final Report, June 1976.

5. E. J. Coyne, The Effect of Microstructure on the Fatigue Behavior of an Aluminum-Lithium Alloy, Ph.D. Thesis, Georgia Institute of Technology, October 1979.

6. T. H. Sanders, Factors Influencing Fracture Toughness and Other Properties of Aluminum-Lithium Alloys, Naval Air Development Center Contract No. N62269-76-C-0271, Final Report, June 1979.

7. K. K. Sankaran, Structure and Properties of Splat Quenched 2024-Type Aluminum Alloys Containing Lithium, Ph.D. Thesis, Massachussetts Institute of Technology, Cambridge, 1978.

8. D. Webster, "Properties and Microstructure of Aluminum-Copper-Magnesium-Lithium Alloys," Met. Trans. A., Vol. 10A, 1979, p. 1913.

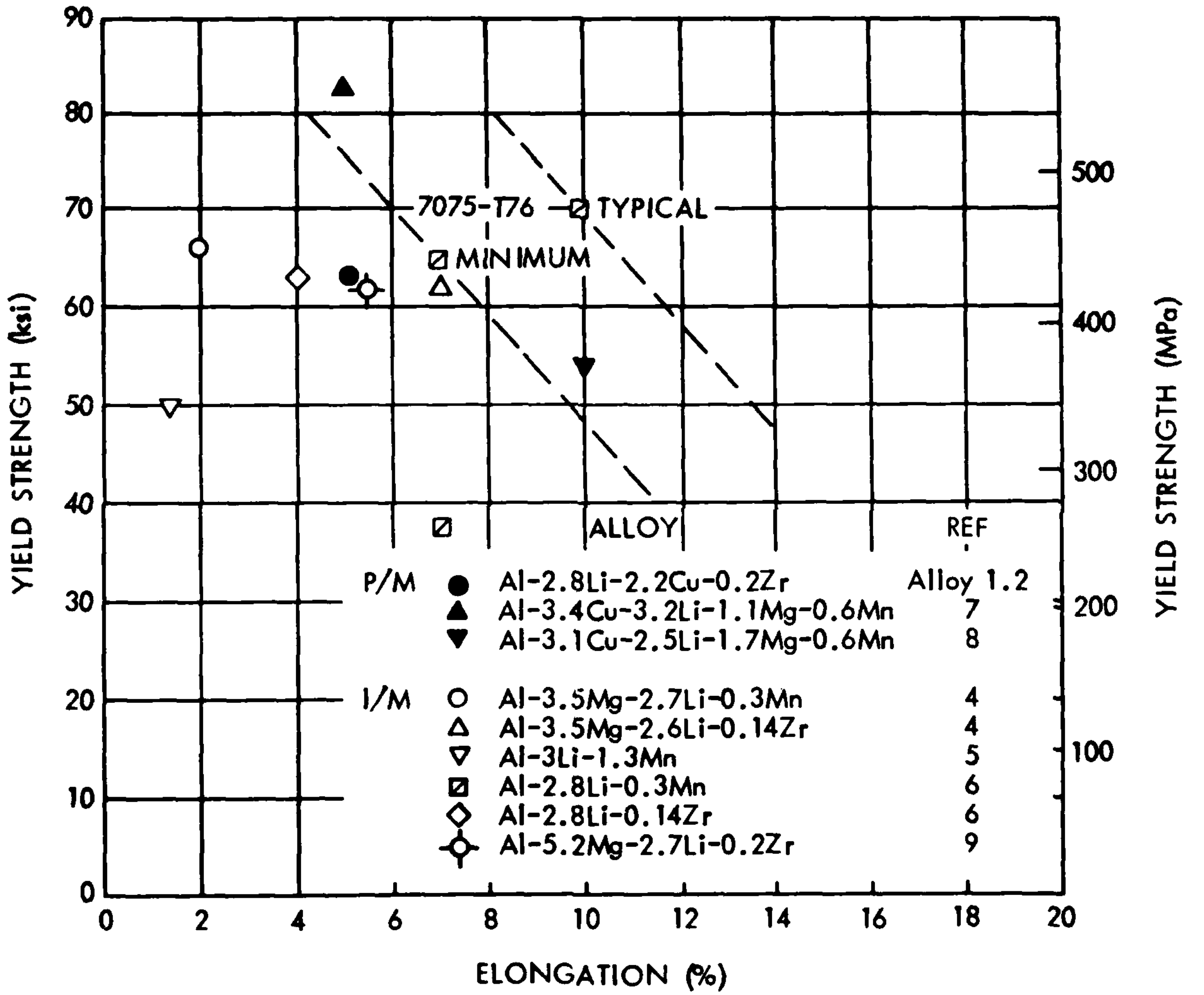

Figure 6. Comparison of tensile properties of P/M and I/M Al-3Li-X alloys, peak-aged condition

10:1 extrusion ratio to a rectangular cross section with an aspect ratio of 8:1. Alloy 1.2 in the present work, which has a yield strength intermediate to these two, was extruded with extrusion ratios of 8:1 or 20:1 to a rectangular cross section with an intermediate aspect ratio of 2:1. A comparison of these results suggests that the extrusion aspect ratio has an important effect on strength, and that the use of axisymmetric extrusions produces significant strength increases as a result of the unique texture developed, different from extrusions of higher aspect ratio.

In future work on the present program, the effect on strength and ductility of varying the aspect ratio of the extrusions will be examined in Alloy 1.2. Also, the effect of adding small amounts of Mg to a modification of Alloy 1.2 will be examined.

2.2 TASK 2 – DEVELOPMENT OF NONLITHIUM-CONTAINING ALLOYS

This task is being conducted by the Alcoa Laboratories.

2.2.1 First-Iteration Alloys

The first iteration alloys are of the nominal compositions shown in Table 4. Splat particulate generated in both air and high purity (low H_2O) argon, as well as fine atomized powder generated in air, were used to produce billets of selected alloys so that the effect of particulate-manufacture process on tensile properties could be assessed. A total of 35 alloy-process variations were examined.

2.2.1.1 Cold Compaction

All of the alloy compositions made with fine atomized powder were isostatically cold compacted by Alcoa's standard wet bag process (Ref. 10). Splat flake compositions were compacted in a different way because of their low apparent density and the tendency of the flakes to cut the rubber bag used in isostatic compaction.

---

10. W. S. Cebulak and D. J. Truax, Program to Develop High Strength Aluminum Powder Metallurgy Products, Phase III–Scale Up A, Contract DAAA25-70-C0358, Final Report, Sept. 29, 1972.

TABLE 4. COMPOSITION OF FIRST-ITERATION OF NONLITHIUM-CONTAINING ALLOYS

Alcoa Alloy Designation	Nominal Composition (wt. %)
2.1A	Al-3.3Fe-3.4Ni-3.4Co
2.2A	Al-3.3Fe-2.3Ni-4.6Co
2.3A	Al-3.3Fe-4.6Ni-2.3Co
2.4A	Al-4.3Fe-5Ni-5Co[a]
2.5A	Al-9.7Mn
2.6A	Al-9.7Mn-2.5Si[a]
2.7A	Al-5Mn-5Si
2.8A	Al-14.2Mn[a]

(a) These alloys have 7.5 atomic percent total solute content; the other alloys have 5.0 atomic percent total solute content.

Splat flakes were cold compacted by using a mechanical die. Multiple disks 2 to 6 cm (1 to 2.5 in.) thick and 11.4-cm (4.5-in.) diameter were produced, exhibiting 50 to 70% of theoretical density. Maximum pressure used was 172 MPa (25 ksi). These compacts were built up to 63.5-cm (25-in.) height and placed in extruded 3003 aluminum alloy cans. The inner diameter was 14 cm (5.5 in.) and can wall thickness was 0.6 cm (0.25 in.). The oversized can facilitates vacuum degassing. Lids were welded to both ends, one end being fitted with a 1.3-cm (0.5 in.)-diameter evacuation pipe. Each cannister was checked for leaks by positively pressurizing the can with argon and using a soap solution to indicate leaks.

2.2.1.2 Hot Consolidation

Five cannisters were processed at one time. Each cannister was connected to a five-port vacuum manifold for an 11 m^3/min (400 cfm) mechanical vacuum pump. The five cannisters were prepumped to 75 μm pressure at room temperature, then moved by a railcar into the preheating furnace. A dynamic vacuum was maintained during the heating cycle. After reaching the set temperature, the compacts were

soaked 1 h; the evacuation tube was then mechanically crimped and welded after the vacuum had stabilized at 75 μm.

Each evacuated cannister was hot pressed to full density producing a 16.5 cm (6.5 in.)-diameter billet. An extrusion cylinder with a closed die was used. The maximum pressure was 1.04 GPa (150 ksi), and the dwell time was five minutes. Subsequently each billet was air cooled to room temperature. The ends were sawed off and the billet machined to 15.6-cm (6.1-in.) diameter. This left a thin, continuous skin of can material to protect the alloy billets, some of which are relatively brittle.

2.2.1.3 Extrusion

The die section is a rectangular shape 1.3 cm x 7 cm (0.5 in. x 2.75 in.) in cross section, giving an extrusion ratio of 24:1. Combinations of hot pressing and extrusion temperatures indicated in Table 5 were used. The billet was crushed in the extrusion cylinder from 15.6 cm (6.1 in.) to 16.5 cm (6.5 in.)-diameter prior to breakout of the extruded shape. In the instances where breakout could not be obtained at the temperature desired (process variations 4 to 8), the crushed billet was removed, air-cooled, remachined to 15.6 cm (6.1 in.) and reextruded at the indicated increased extrusion temperature.

H_2 Content of Extrusions. The H_2 content of the extrusions was found to be related to processing temperature variations (see Table 6). The higher the hot-pressing temperature, and somewhat surprising, the higher the subsequent extrusion temperature, the lower the hydrogen content. The atomized powder alloys have the highest hydrogen content followed by air atmosphere-generated splat alloys and then argon atmosphere-generated splat. As subsequent tensile data show, it is premature to conclude that these levels of hydrogen are detrimental to alloy toughness.

Oxygen content determined by FNA (fast neutron activation) will be reported at a later date.

TABLE 5. THERMAL PROCESSING VARIATIONS USED FOR FIRST-ITERATION NONLITHIUM-CONTAINING ALLOYS

	Temperature	
	Hot Pressing K (°F)	Extrusion K (°F)
Process 1	725 (935)	625 (666)
Process 2	675 (755)	675 (755)
Process 3	675 (755)	625 (666)
Process 4	675 (755)	630 (675)
Process 5	725 (935)	625 (666) + 700 (800)
Process 6	675 (755)	675 (755) + 700 (800)
Process 7	675 (755)	625 (666) + 700 (800)
Process 8	675 (755)	630 (675) + 700 (800)

2.2.1.4 Mechanical Property Tests

Duplicate tensile specimens of each alloy-processing variation were obtained in both L and T orientations. The specimen are of round, threaded-end geometry with a 2.5 cm (1 in.) gage length and 0.5 cm (0.187 in.) gage diameter. There is a shoulder of 0.6-cm (0.25-in.) diameter between the reduced section and threaded end. The results of these tensile tests are presented in Tables 7 and 8. Elastic modulus measurements by the ultrasonic pulse-echo technique are currently being performed. Final selection of the second iteration alloys will be made after these data are available, but preliminary selections based on the better combinations of strength and ductility can now be made.

5 Atomic Percent Solute versus 7.5 Atomic Percent Solute. As expected, an increase in total solute content from 5 atomic percent to 7.5 atomic percent results in an increase in strength and a decrease in both ductility and NTS/YS ratio (see Table 9). The effect of solute content on tensile properties in the Al-Mn system is even more pronounced. In both alloy systems the strength-toughness combination at a total solute level of 7.5 atomic percent is marginally acceptable, at best.

TABLE 6. HYDROGEN CONTENT OF FIRST ITERATION NONLITHIUM-CONTAINING ALLOYS

Alloy	Nominal Composition (w/o)	S No.	Particulate	H Content (ppm)* Process** 1	2	3	5	6	7	8
2.1A	Al-3.3Fe-3.4Ni-3.4Co	513700	Air Splat	1.7	3.9	4.4				
2.2A	Al-3.3Fe-2.3Ni-4.6Co	513682	Atomized Powder	3.8	8.6					
		513702	Air Splat	2.0	2.4	9.2				
		513687	Argon Splat		1.1					
2.3A	Al-3.3Fe-4.6Ni-2.3Co	513701	Air Splat	2.1	4.7	3.1				
2.4A	Al-4.3Fe-5Ni-5Co	513693	Atomized Powder					8.2		
		513697	Air Splat		2.5		1.3		2.5	
2.5A	Al-9.7Mn	513687	Argon Splat		1.0					
		513704	Air Splat	1.8	9.4	12.2				
2.6A	Al-9.7Mn-2.5Si	513666	Atomized Powder	2.2	1.9	6.5				
		513689	Argon Splat	0.5						
		513705	Air Splat	1.1	2.1	4.5				
2.7A	Al-5Mn-5Si	513706	Air Splat	1.5	2.6	2.4				
2.8A	Al-14.2Mn	513678	Atomized Powder		6.3					
		513703	Air Splat	1.2	2.6					2.6
		513658	Air Splat			3.5				

* By total fusion analysis
**See Table 5

TABLE 7. TENSILE AND NOTCHED TENSILE PROPERTIES OF Al-Fe-Ni-Co FIRST ITERATION ALLOYS

Alloy/ S-No.	Process *	Particulate	Orientation	Yield Strength MPa (ksi)	Tensile Strength MPa (ksi)	Elongation (%)	R.A. (%)	NTS/YS
2.1A (Al-3.3Fe-3.4Ni-3.4Co)								
513700-1	1	Air Splat	L	219 (32)	303 (44)	18	40	2.0
			T	225 (33)	303 (44)	12	22	1.9
513700-2	2	Air Splat	L	309 (45)	370 (54)	14	32	1.7
			T	302 (44)	372 (54)	10	18	1.5
513700-3	3	Air Splat	L	299 (43)	369 (53)	13	32	1.7
			T	285 (41)	365 (53)	10	18	1.6
2.2A (Al-3.3Fe-2.3Ni-4.6Co)								
513682-1	1	Atomized Powder	L	264 (38)	350 (51)	15	32	1.9
			T	261 (38)	349 (51)	11	19	1.8
513702-1	1	Air Splat	L	206 (30)	285 (41)	20	42	2.0
			T	208 (30)	285 (41)	16	28	2.0
513682-2	2	Atomized Powder	L	360 (52)	426 (62)	9	18	1.5
			T	356 (52)	430 (62)	9	14	1.3
513687-1	2	Argon Splat	L	236 (34)	314 (46)	18	39	1.9
			T	244 (35)	316 (46)	11	22	1.8
513702-2	2	Air Splat	L	287 (40)	360 (52)	17	40	1.8
			T	283 (41)	359 (52)	10	18	1.7
513703-3	3	Air Splat	L	295 (43)	361 (52)	11	21	1.5
			T	273 (40)	338 (49)	5	9	1.3
2.3A (Al-3.3Fe-4.6Ni-2.3Co)								
513701-1	1	Air Splat	L	201 (29)	291 (42)	18	38	2.0
			T	208 (30)	298 (43)	16	25	1.7
513701-2	2	Air Splat	L	292 (42)	374 (54)	13	31	1.9
			T	294 (43)	379 (55)	9	15	1.6
513701-3	3	Air Splat	L	306 (44)	383 (56)	13	31	1.7
			T	296 (43)	382 (55)	9	16	1.6
2.4A (Al-4.3Fe-5Ni-5Co)								
513693-1X	6	Atomized Powder	L	445 (65)	527 (76)	3	2+	0.6
			T	419 (61)	492 (71)	2	1	0.5
513697-1X	5	Air Splat	L	353 (51)	430 (62)	6	6	1.1
			T	355 (51)	414 (60)	3	2	0.9
513697-2	2	Air Splat	L	512 (74)	550 (80)	3	6	0.6
			T	++	471 (68)	(1.3)	(1)	–
513697-3X	7	Air Splat	L	500 (73)	544 (79)	3.2	4	0.6
			T	506 (73)	527 (76)	1.3	1	0.5

+ Failed outside gage.
++ Failed before 0.2% offset.
* See Table 5.

TABLE 8. TENSILE AND NOTCHED TENSILE PROPERTIES OF Al-Mn AND Al-Mn-Si FIRST ITERATION ALLOYS

Alloy S-No.	Process *	Particulate	Orientation	Yield Strength MPa (ksi)	Tensile Strength MPa (ksi)	Elongation (%)	R.A. (%)	NTS/YS
2.5A (Al-9.7Mn)								
513704-1	1	Air Splat	L	230 (33)	308 (45)	14	28	1.6
			T	228 (33)	301 (44)	6.6	7	1.6
513704-2	2	Air Splat	L	281 (41)	381 (55)	6	8	0.9
			T	268 (39)	365 (53)	2.6	3	0.9
513686-1	2	Argon Splat	L	288 (42)	377 (55)	7.2	12	1.1
			T	290 (42)	365 (53)	3.2	3	1.0
513704-3	3	Air Splat	L	282 (41)	367 (53)	7.2	10	1.2
			T	276 (40)	354 (51)	3.9	2	1.2
2.6A (Al-9.7Mn-2.5Si)								
513666-1	1	Atomized Powder	L	256 (37)	344 (50)	16	28	1.8
			T	257 (37)	348 (50)	14	26	1.7
513689-1	1	Argon Splat	L	187 (27)	252 (37)	21	42	1.9
			T	184 (27)	250 (36)	18	26	2.0
513705-1	1	Air Splat	L	222 (32)	288 (42)	16	33	2.0
			T	226 (33)	291 (42)	20	42	1.9
513705-2	2	Air Splat	L	290 (42)	358 (52)	20	50	1.8
			T	290 (42)	359 (52)	14	28	1.7
513666-2	2	Atomized Powder	L	289 (42)	372 (54)	15	30	1.7
			T	284 (41)	379 (55)	12	21	1.6
531705-3	3	Air Splat	L	305 (44)	364 (53)	18	45	1.7
			T	292 (42)	364 (53)	16	34	1.7
513666-3	3	Atomized Powder	L	312 (45)	390 (57)	14	32	1.6
			T	312 (45)	396 (57)	13	22	1.5
2.7A (Al-5Mn-5Si)								
513706-1	1	Air Splat	L	172 (25)	238 (34)	26	56	2.1
			T	169 (24)	236 (34)	24	45	2.1
513706-2	2	Air Splat	L	210 (30)	287 (42)	24	50	2.0
			T	205 (30)	284 (41)	15	27	2.0
513706-3	3	Air Splat	L	232 (34)	301 (44)	20	47	1.9
			T	223 (32)	297 (43)	14	27	2.0
2.8A (Al-14.2Mn)								
513703-1	1	Air Splat	L	302 (44)	405 (59)	3.9	5	0.9
			T	306 (44)	390 (57)	2.6	3	0.9
513703-2	2	Air Splat	L	+	399 (58)	+	+	–
			T	+	363 (53)	+	+	–
513678-2	2	Atomized Powder	L	433 (63)	503 (73)	1.3	1	0.5
			T	451 (65)	472 (68)	1.3	1	0.5
513658-1	3	Air Splat	L	461 (67)	496 (72)	1.3	1	0.4
			T	+	383 (56)	+	+	+
513708-3X	8	Air Splat	L	+	442 (64)	+	+	+
			T	+	351 (51)	+	+	+

+ Failed before 0.2% offset.
* See Table 5.

TABLE 9. EFFECT OF SOLUTE LEVEL ON TENSILE AND NOTCHED TENSILE PROPERTIES ON Al-Fe-Ni-Co AND Al-Mn FIRST-ITERATION ALLOYS

Alloy No.	S-No.	Process*	Solute Level (at. %)	Particulate	Yield Strength MPa (ksi)	Tensile Strength MPa (ksi)	Elongation (%)	R.A. (%)	NTS/YS
Al-Fe-Ni-Co									
2.1A	513700-2	2	5.0	Air Splat	309 (45)	370 (54)	14	32	1.7
2.4A	513697-2	2	7.5	Air Splat	512 (74)	550 (80)	3	6.0	0.6
Al-Mn									
2.5A	513704-3	3	5.0	Air Splat	282 (41)	367 (53)	7	10	1.2
2.8A	513558-1	3	7.5	Air Splat	461 (67)	495 (72)	1.3	1	0.4

*See Table 5

Addition of Si to Al-Mn Alloys. One consideration in alloy design for this program is the effect of changing identity of the precipitated phase(s). In the Al-Mn system this involves varying the thermal history to produce $Al_{12}Mn$ or Al_6Mn and adding Si to change the precipitated phases to $Al_{12}Mn_3Si$ with possible precipitation of free Si. Table 10 shows the dramatic effect of Si on tensile properties of an alloy containing 7.5 atomic percent total solute. Although the toughness-ductility of Al-7.5 at.% Mn is unacceptable, the toughness-ductility of Al-7.5 at.% (Mn + Si) is good. This alloy has 50% higher solute content than alloy 2.8A (Al-5 at.% Mn, S No. 513686-1), yet it has significantly better ductility and toughness as measured by the NTS/YS ratio. These results suggest that a total (Mn + Si) solute content higher than 7.5 at.% may result in an even higher strength and with acceptable toughness and ductility.

These effects described above may be attributable to precipitated phase identity as revealed by Guinier analysis of the extrusions (see Table 11). Conclusive proof of this must await further microstructural characterization.

TABLE 10. EFFECT OF Si ADDITION ON TENSILE AND NOTCHED TENSILE PROPERTIES OF AL-Mn FIRST-ITERATION ALLOYS

Alloy No.	S-No.	Process*	Mn (Wt. %)	Si (Wt. %)	Particulate	Yield Strength MPa (ksi)	Tensile Strength MPa (ksi)	Elongation (%)	R.A. (%)	NTS/YS
5 Atomic Percent Total Solute										
2.5A	513704-3	3	9.2	–	Air Splat	282 (41)	367 (53)	7.2	10	1.2
2.7A	513706-3	3	5.0	5.0	Air Splat	232 (34)	309 (44)	20	47	1.9
7.5 Atomic Percent Total Solute										
2.6A	513705-3	3	9.7	2.4	Air Splat	305 (44)	364 (53)	18	45	1.7
2.8A	513658-1	3	14	–	Air Splat	461 (67)	495 (72)	1.3	1	0.4

*See Table 5

The Effect of Air and Argon Atmosphere During Splat Generation. A comparison of tensile properties of splat alloys generated in air or argon atmospheres and then extruded is presented in Table 12. Comparison is presented for a relatively low strength alloy, 2.6A, and two higher strength alloys, 2.2A and 2.5A. These results show that the splat alloys produced in an argon atmosphere exhibit a marginally higher toughness (NTS/YS) and tensile ductility, and a lower strength. Results of surface oxide character previously presented (Ref. 3) showed that these alloy systems are reasonably stable against excessive oxidation during particulate generation in an air atmosphere. This finding may explain why the argon atmosphere did not improve particulate bonding. However, the use of an argon atmosphere for particulate generation does affect the hydrogen content; see Table 6. In summary, the extrusions made from splat produced in an argon atmosphere offers no significant advantage of tensile properties for these alloys over those made in an air atmosphere.

The Effect of Splat Particulate and Fine Atomized Powder. A comparison of tensile properties of alloys made from splat particulate generated in an air atmosphere and fine atomized powder generated in air is presented in Table 13. Intuitively, one may expect that particulate type may affect the anisotropy in tensile properties.

TABLE 11. RESULTS OF GUINIER AND PINHOLE DIFFRACTION (TEXTURE) ANALYSES OF FIRST ITERATION NONLITHIUM-CONTAINING ALLOYS

Alloy No. S-No.	Process*	Amount of Phases Present $Al_9(FeNiCo)_2$	$MnAl_6$	$MnAl_{12}$	Mn_3SiAl_{12}	Si	Texture
2.1A (Al-3.3Fe-3.4Ni-3.46)							
513700-1	1	Large					Predominately rolling texture
513700-2	2	Large					
513700-3	3	Large					
2.2A (Al-3.3Fe-2.3Ni-4.6Co)							
513702-3	3	Medium+					Predominately rolling texture
2.4A (Al-4.3Fe-5Ni-5Co)							
513697-1X	6	Large					Low degree of preferred orientation
513697-2	5	Large					
513697-3X	2	Large					
2.5A (Al-9.7Mn)							
513704-1	1		Large	Small			Predominately rolling texture
513704-2	2		Large	Medium			
513704-3	3		Large	Small+			
2.6A (Al-9.7Mn-2.5Si)							
513666-2	2				Large		Predominately rolling texture
513705-1	1				Large		
513705-2	2				Large		
513705-3	3				Large		
2.7A (Al-5Mn-5Si)							
513706-1	1				Large	Med.	Predominately rolling texture
513706-2	2				Large	Med.	
513706-3	3				Large	Med.	
2.8A (Al-14.2Mn)							
513658-1	3		Large	Small			Low degree of preferred orientation
513703-3X	8		Large	Med.			

*See Table 5

TABLE 12. EFFECT OF SPLAT-MAKING ATMOSPHERE ON TENSILE AND NOTCHED TENSILE PROPERTIES OF Al-Fe-Ni-Co, Al-Mn, AND Al-Mn-Si ALLOYS

Alloy No. (w/o)	Process*	Orientation	Splat-Making Atmosphere	Yield Strength MPa	Yield Strength (ksi)	Tensile Strength MPa	Tensile Strength (ksi)	Elongation (%)	R.A. (%)	NTS/YS
2.2A (Al-3.3Fe-2.3Ni-4.6Co)										
513687-1	2	L	Argon	236	(34)	314	(46)	18	39	1.9
		T		244	(35)	316	(46)	11	22	1.8
513702-1	2	L	Air	287	(42)	360	(52)	17	40	1.8
		T		283	(41)	359	(52)	10	18	1.7
2.5A (Al-9.7Mn)										
513686-1	2	L	Argon	287	(42)	377	(55)	7.2	12	1.1
		T		290	(42)	365	(53)	3.2	3	1.0
513704-2	2	L	Air	280	(41)	381	(55)	6	8	0.9
		T		268	(39)	365	(53)	2.6	3	0.9
2.6A (Al-9.7Mn-2.5Si)										
513689-1	1	L	Argon	187	(27)	252	(37)	21	42	1.9
		T		183	(26)	250	(36)	18	26	2.0
	1	L	Air	222	(32)	288	(42)	16	33	2.0
		T		228	(33)	291	(42)	20	42	1.9

*See Table 5

TABLE 13. EFFECT OF PARTICULATE TYPE ON TENSILE PROPERTIES OF Al-Fe-Ni-Co AND Al-Mn-Si ALLOYS

Alloy No. (w/o) S-No.	Process*	Particulate Type**	Orientation	Yield Strength MPa	Yield Strength (ksi)	Tensile Strength MPa	Tensile Strength (ksi)	Elongation (%)	R.A. (%)	NTS/YS
2.2A (Al-3.3Fe-2.3Ni-4.6Co)										
513682-1	1	P	L	264	(38)	350	(51)	15	32	1.9
			T	261	(38)	349	(51)	11	19	1.8
513702-1	1	S	L	206	(30)	285	(41)	20	42	2.0
			T	208	(30)	285	(41)	16	28	2.0
2.6A (Al-9.7Mn-2.5Si)										
513666-1	1	P	L	256	(37)	344	(50)	16	28	1.8
			T	257	(37)	348	(50)	14	26	1.7
513705-1	1	S	L	222	(32)	288	(42)	16	33	2.0
			T	226	(33)	291	(42)	19	42	1.9
513666-2	2	P	L	289	(42)	372	(54)	15	30	1.7
			T	284	(41)	379	(55)	12	21	1.6
513705-2	2	S	L	290	(42)	358	(52)	20	50	1.8
			T	290	(42)	359	(52)	14	28	1.7
513666-3	3	P	L	312	(45)	390	(57)	14	32	1.6
			T	312	(45)	396	(57)	13	22	1.5
513705-3	3	S	L	305	(44)	364	(53)	18	45	1.7
			T	292	(42)	364	(53)	16	34	1.7

* See Table 5
**P = fine atomized powder produced in air,
S = Splat produced in air

In the present study, tensile properties were assessed only in the L and T directions, because of the limiting size of the extrusion. As shown in the table, the tensile property variation between L and T orientations is unaffected by particulate form. However, the extrusions made from atomized powder consistently exhibit a higher yield and tensile strength and lower elongation, reduction of area, and NTS/YS ratio compared to those made from splats. The changes in tensile ductility and NTS/YS ratio are accompanied by changes in macroscopic fracture morphology. Tensile specimens of the atomized powder alloys typically exhibit a smooth and flat fracture appearance except for shear lips while the alloys made from splat alloys typically exhibit a rougher fracture surface morphology not unlike that of the fracture appearance of a laminated composite.

The Effect of Thermal Process History. The processing conditions used in the first iteration alloy extrusions were selected on the basis of certain precipitate phases expected in alloys 2.5A through 2.8A and the intention to minimize structural coarsening in alloys 2.1A through 2.4A, as discussed previously (Ref. 3). The process variations are listed in Table 5. Processes 4 through 8 are the consequence of the inability to extrude some of the alloys at 625 K (666°F) or 675 K (755°F). In the analysis following, only processes 1, 2, and 3 are considered. The Al-Fe-Ni-Co alloys (2.1A through 2.4A) and the Al-Mn-Si alloys (2.5A through 2.8A) do not always exhibit optimum strength for the same processing condition.

In Tables 7 and 8, the influence on tensile properties of reduced hot pressing temperature with a constant extrusion temperature can be seen (for each alloy, compare process 1 with process 3). In both the Al-Fe-Ni-Co and Al-Mn-Si alloy systems, a substantial increase in strength is obtained by the use of a lower hot pressing temperature. This strength increase is accompanied by a ductility and toughness decrease. This lower ductility and toughness is acceptable except in Alloys 2.4A and 2.8A. Although microstructural analysis has not been completed, the lower strength of the alloys hot-pressed at the higher temperature is believed to be attributable to the coarser precipitated second phases and subgrain sizes.

From these same tables, a comparison of tensile properties for process 2 and process 3 indicates the influence of reduced extrusion temperature with a constant hot pressing temperature. In the Al-Fe-Ni-Co alloys, the lower extrusion temperature of process 3 gave a yield strength about 7 MPa (1 ksi) more than the higher extrusion temperature (process 2) except for alloy 2.1A, where process 2 produced the higher strength. Both processes 2 and 3 produced essentially the same strength level, but the tensile ductility of process 2 is better than process 3. Since the flow stress is lower during a higher temperature extrusion, process 2 is more practical for the Al-Fe-Ni-Co alloys.

In the Al-Mn and Al-Mn-Si alloys, results similar to the Al-Fe-Ni-Co alloys were observed; namely, the lower extrusion temperature gave higher strength than the higher extrusion temperature. These results are consistent with those reported by Sanders et al. for somewhat similar alloys being developed for elevated temperature applications (Ref. 11). In contrast with the Al-Fe-Ni-Co alloys, however, the ductility of these alloys was not altered by the change in process condition.

A list of alloy-process conditions exhibiting the best strength-toughness combinations is presented in Table 14. The highest yield strength is exhibited by alloy 2.4A, 511 MPa (74 ksi), with a corresponding NTS/YS ratio of 0.6. Disregarding all notch-sensitive alloys, i.e., all alloys whose NTS/YS <1.0, the highest yield strength is 360 MPa (52 ksi) with a corresponding NTS/YS ratio of 1.5, exhibited by alloy 2.2A, Al-3.3Fe-2.3Ni-4.6Co, and which was produced as an atomized powder alloy by the intermediate thermal processing condition. This particular alloy was not produced using the lowest-temperature processing condition which may result in a slightly higher strength. Four other alloys were produced by the low-temperature processing, but they exhibit strengths about 10% lower and NTS/YS ratios about 10 to 15% higher than alloy 2.2A. In general, the Al-Fe-Ni-Co alloys exhibit a higher strength

---

11. R. E. Sanders, G. J. Hildeman, and D. J. Lege, Elevated Temperature Alloy Development, Alcoa Annual Technical Report on Air Force Contract F33615-77-C-5086, March 1979.

TABLE 14. SUMMARY OF TENSILE PROPERTIES FOR TEN BEST FIRST-ITERATION NONLITHIUM-CONTAINING ALLOYS, LISTED IN ORDER OF DECREASING STRENGTH

Alloy No.	S-No.	Process*	Particulate Type	Yield Strength MPa (ksi)	Tensile Strength MPa (ksi)	Elongation (%)	R.A. (%)	NTS/YS
2.4A	513697-2	2	Air Splat	512 (74)	550 (80)	3	6	0.6
2.8A	513658-1	3	Air Splat	461 (67)	495 (72)	1.3	1	0.4
2.2A	513682-2	2	Atomized Powder	360 (52)	426 (62)	9.2	18	1.5
2.6A	513666-3	3	Atomized Powder	312 (45)	390 (57)	14	32	1.6
2.1A	513700-2	2	Air Splat	309 (45)	370 (54)	14	32	1.7
2.3A	513701-3	3	Air Splat	306 (44)	383 (56)	13	31	1.7
2.6A	513705-3	3	Air Splat	305 (44)	364 (53)	18	45	1.7
2.5A	513686-1	2	Argon Splat	288 (42)	377 (44)	7.2	12	1.1
2.5A	513704-3	3	Air Splat	282 (41)	366 (53)	7.2	10	1.2
2.7A	513706-3	3	Air Splat	231 (34)	301 (45)	20	47	1.9

*See Table 5

than the Al-Mn-Si alloys. The tensile properties of alloy 2.4A suggest that further improvement in useful strength by increasing total solute content much above 5 atomic percent in the Al-Fe-Ni-Co alloys is not fruitful.

Tensile properties of alloy 2.6A are significant in that strength levels comparable to the Al-Fe-Ni-Co alloys are achieved. Depending on the elastic modulus determination, solute additions in excess of 7.5 atomic percent in the Al-Mn-Si alloy system may offer an additional strength increase than the first iteration alloys when processed similarly.

As shown in Table 7, the high Ni version of the Al-Fe-Ni-Co air splat alloys fabricated by the intermediate or low-temperature thermal processing has a slight advantage over the high Co version processed similarly. Alloy 2.3A was not processed in atomized powder form. If it were processed in powder form, and were processed by optimum thermal processing techniques similar to that used for alloy 2.2A, a yield strength of about 373 MPa (54 ksi) and with good ductility may be achieved. If so, this would probably be the highest strength-ductility combination of any of the Al-Fe-Ni-Co alloys having a total solute content of 5 atomic percent.

From the tensile data in Table 8 for the Al-Mn and Al-Mn-Si alloys, one can conclude that the lower strength of the alloy 2.6A at equivalent solute level of alloy 2.8A is due to a difference in volume fraction of second-phase precipitates. The higher strength of Alloys 2.5A and 2.8A in the intermediate thermal processing condition can be attributed to the presence of both $Al_{12}Mn$ and Al_6Mn, while Alloy 2.6A has only $Al_{12}Mn_3Si$, which must occur in a lower volume fraction.

2.3 TASK 3 – QUANTITATIVE MICROSTRUCTURAL ANALYSIS AND MECHANICAL PROPERTY CALCULATIONS

Task 3 is being conducted by the Georgia Institute of Technology.

All of the results summarized in this report section are taken from studies on Al-Li Alloys 1.2 (Al-3Li-2Cu-0.2Zr) and 1.6 (Al-3Li-1.5Mn). These alloys were made from argon atomized splat, screened, vacuum hot-pressed, then extruded to a rectangular cross section with an extrusion ratio of 8:1. TEM studies were conducted on either solution-heat-treated (SHT) or SHT and aged material to characterize the microstructure. Tensile tests on round samples were performed to determine the tensile properties (dimensions of the gage section: 20-mm length, 4-mm diameter). Specimen orientation was longitudinal (specimen axis parallel to extrusion direction). Scanning electron microscopy (SEM) studies were carried out on fractured tensile samples to obtain information concerning crack nucleation and crack propagation modes.

2.3.1 Microstructural Characterization

TEM foils were prepared using a twin-jet electropolishing apparatus. Preparation of useful thin foils from the extruded splat material is rather difficult because of preferred attack of the electrolyte along prior flake (splat) boundaries. Figure 7a shows a SEM of an electrolytically polished surface where the flake boundaries are clearly visible, while in Fig. 7b the flake boundary is shown as it appears in a TEM micrograph. Moreover, the foils have to be examined immediately after preparation since a surface film starts forming on the foil surfaces when exposed to ambient air. This surface film effect is more pronounced in Alloy 1.6 than in Alloy 1.2.

<u>Alloy 1.2 (Al-3Li-2Cu-0.2Zr).</u> The subgrain size ranges from 2 to 4 μm (Fig. 8). Because of the relatively sharp texture in this alloy (Ref. 3), it is often difficult to differentiate between subgrain boundaries and high-angle boundaries. Within the subgrains, low-angle boundaries were frequently observed in which individual dislocations could easily be resolved. Also, some larger particles were found along

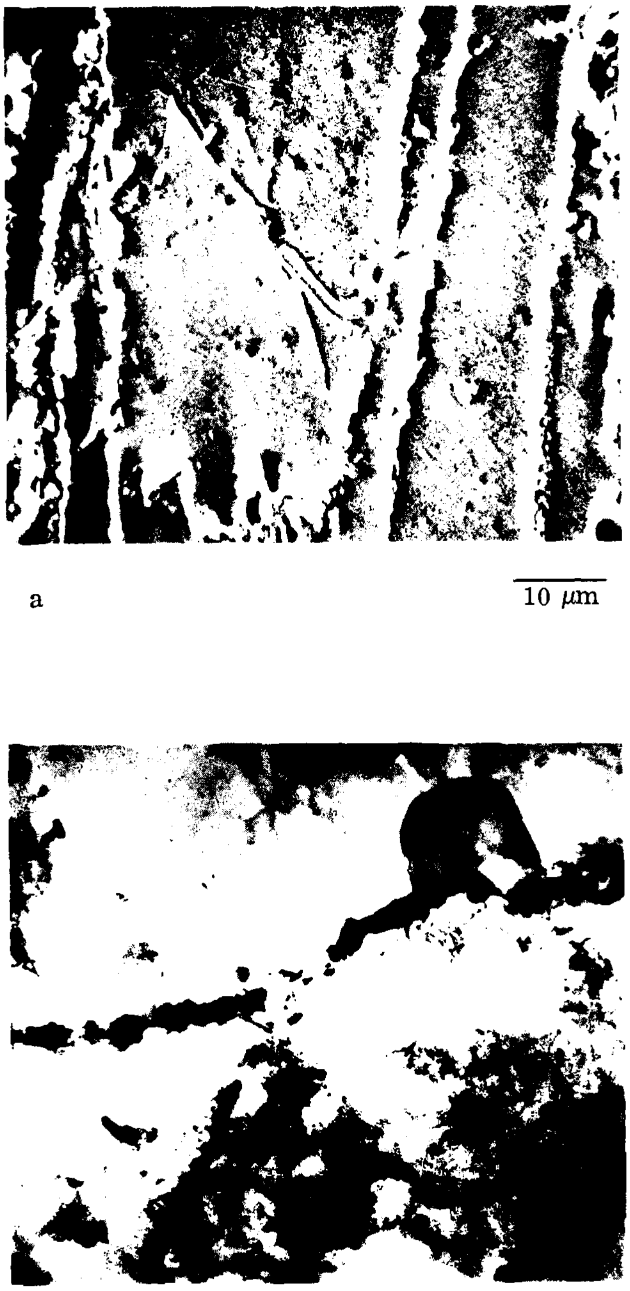

a 10 μm

b 1.0 μm

Figure 7. (a) Flake boundaries on electropolished surface of Alloy 1.2 (*Al-3Li-2Cu-0.2Zr*) (*SEM*).
(b) Flake boundary in thin foil of Alloy 1.6 (Al-3Li-1.5Mn) (TEM).

Figure 8. Subgrain structure in Alloy 1.2 (Al-3Li-2Cu-0.2Zr) (TEM).

subgrain and/or grain boundaries (see arrows in Fig. 8, which are not identified as yet).

Microstructural changes were studied in material aged at 473 K (392° F) for 0.75 h (underaged), 8 h (peak-aged) and 100 h (overaged). In the underaged condition, metastable δ'-precipitates were observed with sizes between 100 Å and 300 Å, as shown in the dark field micrograph (Fig. 9a). A quantitative analysis of the size distribution of the δ'-precipitates has not been performed so far. The δ'-precipitates are spherical in shape and the volume fraction seems to be rather high. Overlapping of the individual precipitates makes it difficult to measure their sizes precisely. Precipitate-free zones (PFZ) along grain boundaries can also be seen in Fig. 9a and more clearly in the bright field micrograph in Fig. 9b. The width of the PFZs (both sides of the grain boundary) is approximately 0.1 to 0.15 μm. No precipitates were found along grain or subgrain boundaries, as shown in Fig. 9b, other than the larger particles mentioned above. This suggests that the PFZs are the result of vacancy-depleted rather than alloy-depleted zones. Only a few precipitates of the θ'-phase were found in the underaged condition. Those which were observed seemed to be connected to dislocation lines which are present in the alloy after quenching from the solution temperature (see Fig. 9b). The maximum length of traces of the θ'-precipitates in Fig. 9b is approximately 0.15 μm and the thickness of the platelets is estimated to be about 50 Å.

After aging for 8 h (peak-aged condition), the size of the δ'-precipitates increased to about 300 Å to 500 Å, as shown in the dark field micrographs in Figs. 10a and 10b. The shape is still spherical, as observed in the underaged condition. The width of the PFZs increased slightly to about 0.2 μm. Within the matrix, larger precipitates of θ' can be seen in the peak-aged condition (Fig. 11a). Now, the maximum length of the platelet traces is approximately 1 μm, while the thickness has increased to about 100 Å. The distribution of the θ'-platelets appears to be rather inhomogeneous, as shown in Fig. 11b, which was taken from a slightly deformed tensile specimen. A large number of small θ'-platelets are frequently found along low-angle boundaries (arrows in Fig. 11b), with platelet trace lengths of approximately 0.15 μm. The

a 0.2 μm

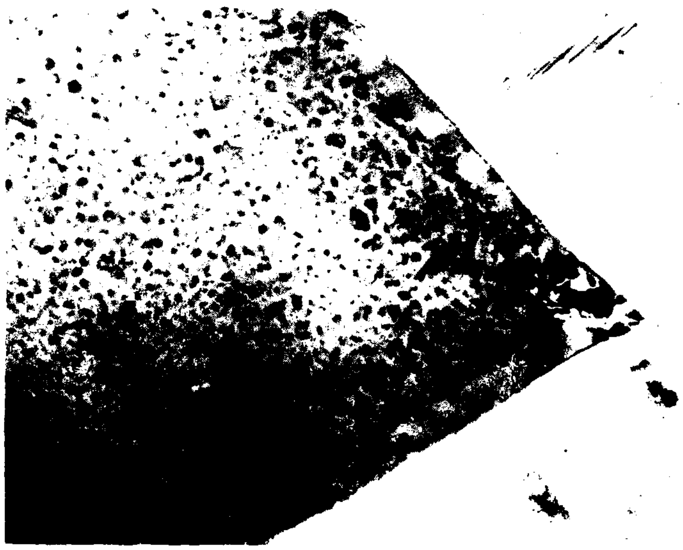

b 0.2 μm

Figure 9. Alloy 1.2 (Al-3Li-2Cu-0.2Zr) in underaged condition (0.75 h, 473 K) (TEM):
(a) dark-field micrograph using (100) δ'-reflection,
(b) bright-field micrograph.

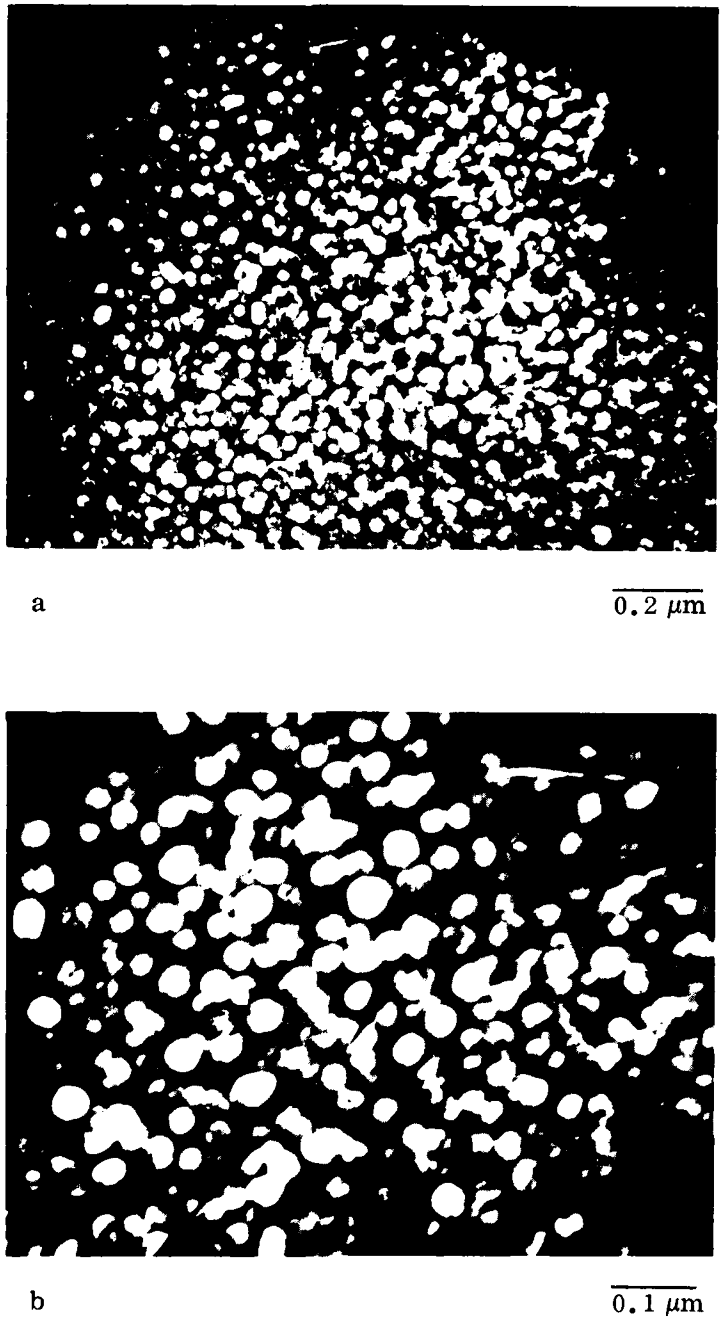

Figure 10. Alloy 1.2 (Al-3Li-2Cu-0.2Zr), peak-aged condition (8 h, 473 K) (TEM):
(a) and (b) dark-field micrographs showing δ'-precipitates.

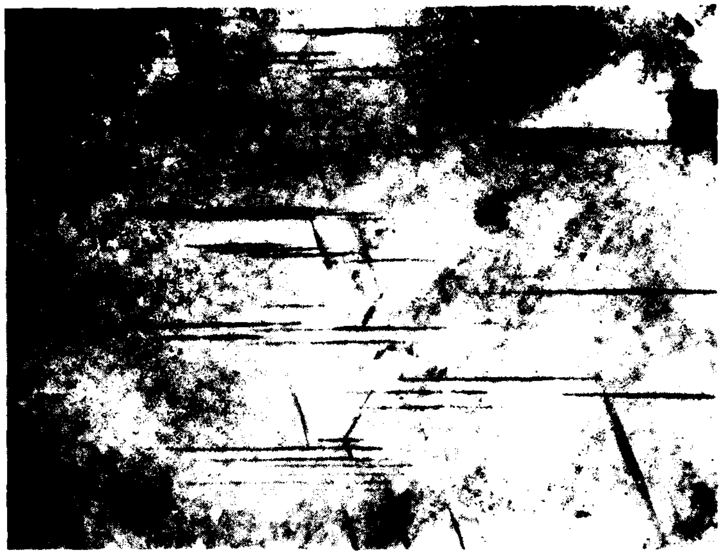

a 0.5 μm

b 0.5 μm

Figure 11. Alloy 1.2 (Al-3Li-2Cu-0.2Zr), peak-aged condition (8 h, 473 K) (TEM):
(a) and (b) bright-field micrographs showing size and distribution of θ'-precipitates.

maximum trace length of the θ'-platelets in the overaged [473 K (392° F), 100 h] condition is approximately the same as in the peak-aged condition (~ 1 μm), while the thickness has increased slightly to about 150 Å. (See Figs. 12a and b.) The micrograph in Fig. 12a shows traces of three different θ' orientations, while Fig. 12b shows two orientations.

Alloy 1.6 (Al-3Li-1.5Mn). The subgrain size in this alloy is approximately 4 μm, similar to that for Alloy 1.2. This is shown in the micrograph in Fig. 13. It was also observed that the Mn-rich particles in this alloy exhibit a significant size distribution. The larger particles are approximately 1 μm in diameter, while the smaller ones range in size from 0.1 to 0.5 μm. This result is somewhat surprising, since in rapidly solidified P/M products, the larger particles should not be observed at all. These new finding are in variance with results reported previously (Ref. 3), where only the small Mn-rich particles were observed (Fig. 37 of Ref. 3). Accordingly, thin foils of Alloy 1.6 of the unscreened material (Extrusion No. 1.6-2) and the screened material (Extrusion No. 1.6A-1) were reexamined. Figure 14 shows a micrograph of the unscreened material at lower magnification. Here, too, a particle-size distribution is seen to be similar to that observed previously for the screened material. However, the ratio of small-to-large particles seems slightly higher for the unscreened material. (Compare Figs. 13 and 14.) The micrographs in Fig. 15a (screened material) and Fig. 15b (unscreened material) show typical particle distributions and sizes at a higher magnification.

The microstructural changes upon aging Alloy 1.6 at 473 K were also studied for 0.75-h, 8-h, and 100-h aging time. In the underaged condition (0.75 h), spherical δ'-precipitates were found with diameters of approximately 200 Å, as can be seen from the dark field micrograph in Fig. 16. PFZs were also observed along grain boundaries, similar to Alloy 1.2. The width of these denuded zones is about 0.1 to 0.15 μm (see Fig. 17). In the peak-aged condition, the δ'-precipitate size increased to about 300 Å to 400 Å, as shown in Fig. 18. This dark field micrograph also shows PFZs around Mn-rich particles of approximately 0.1 μm. As shown in Fig. 19a, the PFZs along high-angle boundaries measured about 0.15 to 0.2 μm, while some of the subgrain boundaries do not exhibit PFZs; see Fig. 19b.

a 0.2 μm

b 0.2 μm

Figure 12. Alloy 1.2 (Al-3Li-2Cu-0.2Zr), overaged condition (100 h, 473 K) (TEM):
(a) and (b) bright-field micrographs showing θ'-precipitates.

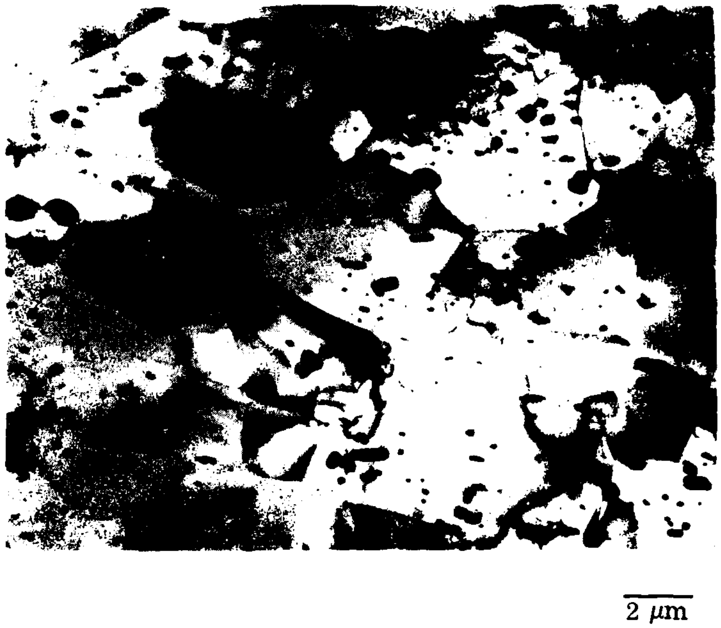

Figure 13. Alloy 1.6 (Al-3Li-1.5Mn) made from screened particulates, SHT condition, showing Mn-rich particles (TEM).

Figure 14. Alloy 1.6 (Al-3Li-1.5Mn) unscreened particulates in SHT condition showing Mn-rich particles (TEM).

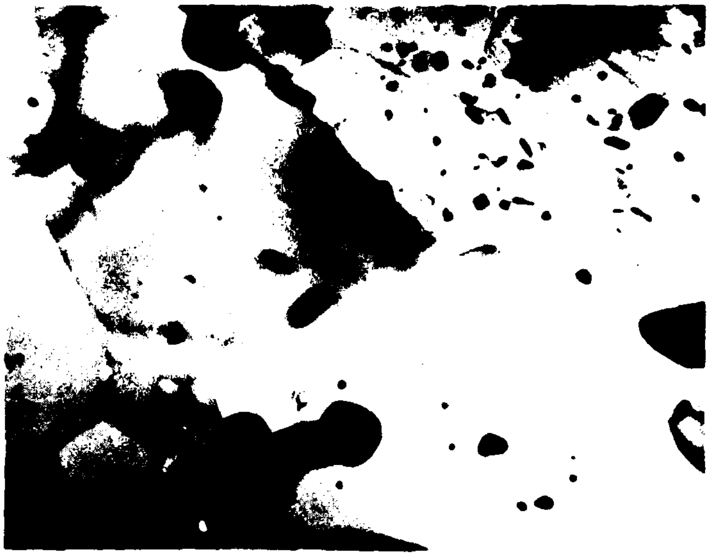

a 1.0 μm

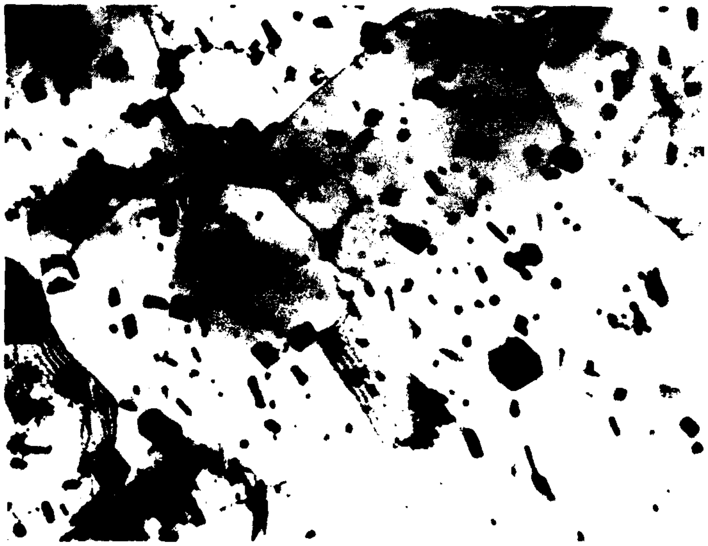

b 1.0 μm

Figure 15. Alloy 1.6 (Al-3Li-1.5Mn), particle size and distribution (TEM):
(a) screened particulates;
(b) unscreened particulates.

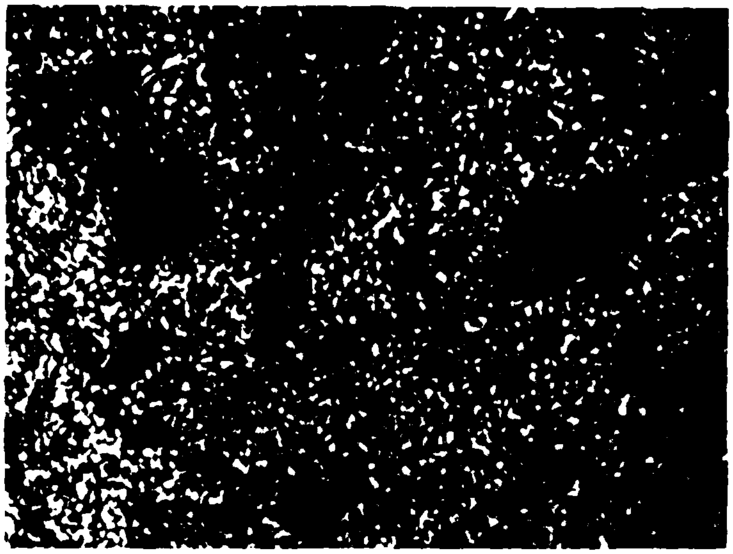

0.2 μm

Figure 16. Alloy 1.6 (Al-3Li-1.5Mn), underaged condition (0.75 h, 473 K) (TEM).
Dark-field micrograph using (100) δ'-reflection.

0.2 μm

Figure 17. Alloy 1.6 (Al-3Li-1.5Mn), underaged condition (0.75 h, 473 K) (TEM).
Bright-field micrograph showing precipitate free zone.

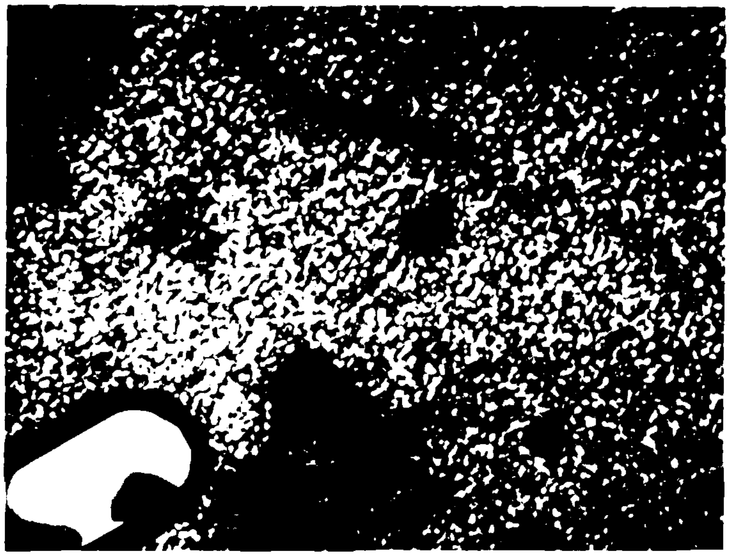

0.5 μm

Figure 18. Alloy 1.6 (Al-3Li-1.5Mn), peak-aged condition (8 h, 473 K) (TEM).
Dark-field micrograph using (100) δ'-reflection.

a 0.2 μm

b 0.2 μm

Figure 19. Alloy 1.6 (Al-3Li-1.5Mn), peak-aged condition:
(a) PFZ along high-angle grain boundary;
(b) subgrain boundary without PFZ.

TEM studies have been conducted in Alloy 1.2 at an aging temperature of 453 K (356° F) only for the underaged condition (1 h). It was found that the δ'-precipitate size is smaller than that observed at an aging temperature of 473 K (392° F). The dark field micrographs in Figs. 20a and b revealed diameters of less than 100 Å, while diameters of 100 Å to 300 Å were found at 473 K aging temperature (compare with Fig. 9a). The number of θ'-precipitates appears to be slightly higher at the lower aging temperature. Most of the θ'-precipitates are connected either to dislocation lines within the matrix or to low-angle boundaries.

2.3.2 Tensile Properties

The variation of yield strength $\sigma_{0.2}$, true fracture strength σ_f, and plastic elongation (strain) to fracture ϵ_f as a function of aging time at 473 K is plotted in Fig. 21 for Alloy 1.2 and in Fig. 22 for Alloy 1.6. The numerical data are summarized in Table 15. The yield strength increases slightly for both alloys between the underaged and the peak-aged condition, but drops sharply upon overaging. The plastic strain to fracture decreases between underaged and peak-aged conditions and then slightly increases for the overaged condition. All specimens in the underaged and peak-aged conditions failed without necking, while some of the overaged samples showed a slight necking. In all cases, the measured values for the elongation were lower than the target value of 10%, with only Alloy 1.6 in the underaged condition meeting the 7% minimum acceptable value.

Additional tensile tests on the peak-aged condition in both alloys were performed to study the effects of different environmental and heating-up conditions for solution heat treatment. Three heat-treatment procedures were used: in air, in vacuum, and in lead bath. Also, two different specimen surface treatments were studied for Alloy 1.2. One set of specimens was mechanically polished (1-μm diamond paste),

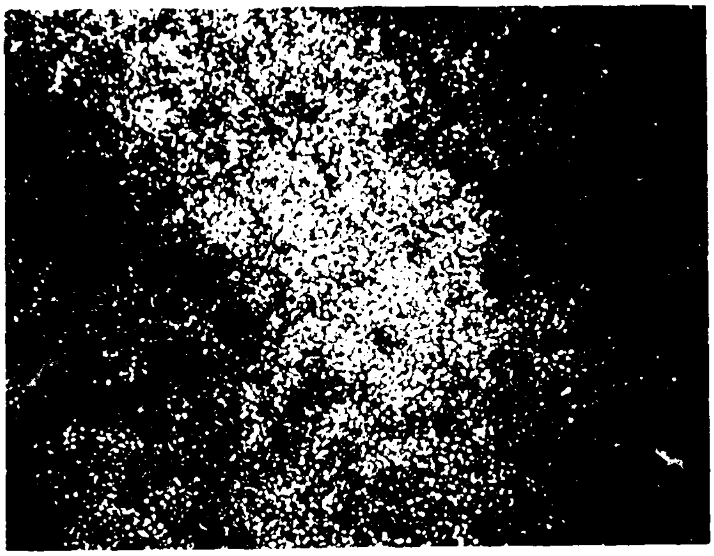

a 0.2 μm

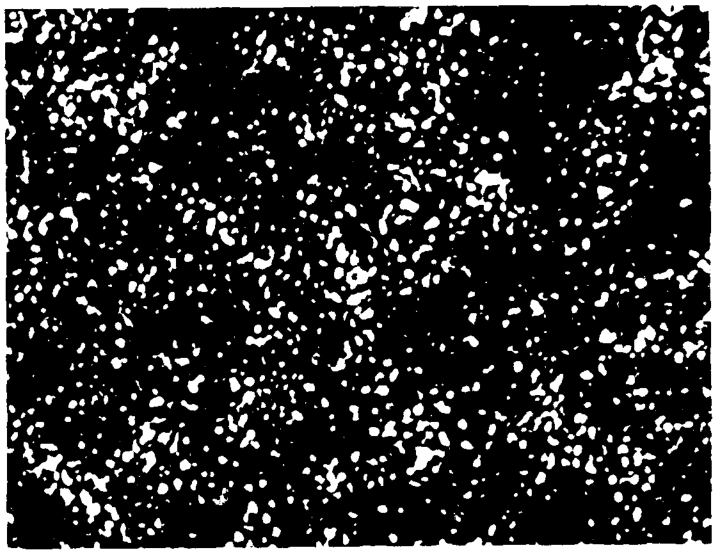

b 0.1 μm

Figure 20. Dark-field micrographs of Alloy 1.2 (Al-3Li-2Cu-0.2Zr) in underaged condition (1 h, 453 K) using (100) δ'-reflection (TEM).

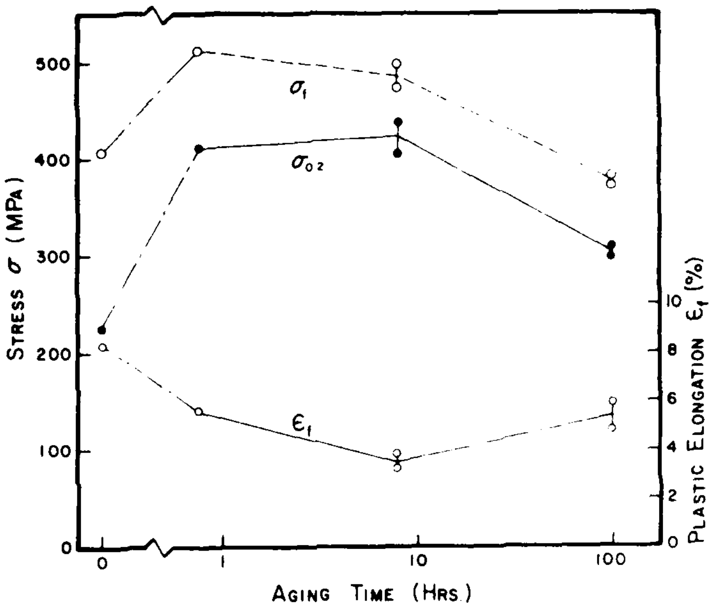

Figure 21. Tensile properties of Alloy 1.2 (Al-3Li-2Cu-0.2Zr) as a function of aging time at 473 K.

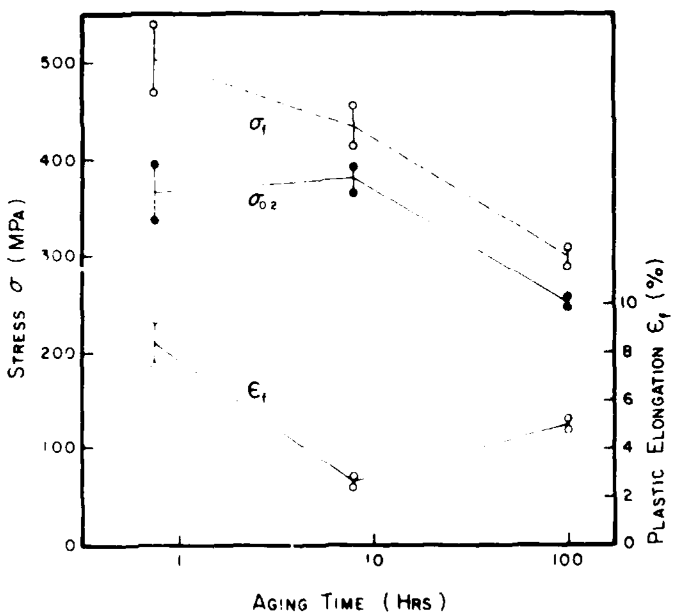

Figure 22. Tensile properties of Alloy 1.6 as a function of aging time at 473 K.

TABLE 15. TENSILE PROPERTIES OF ALLOYS 1.2 AND 1.6 FOR VARIOUS AGING TIMES AT 473 K (392° F)

Alloy No.	Aging Time at 473 K (h)	$\sigma_{0.2}$ MPa (ksi)	σ_f MPA (ksi)	ϵ_f (%)
1.2 (Al-3Li-2Cu-0.2Zr)	0.75	411 (60)	511 (74)	5.6
	8	403 (58)	473 (69)	3.8
		437 (63)	497 (72)	3.2
	100	298 (43)	381 (55)	5.9
		308 (45)	373 (54)	4.8
1.6 (Al-3Li-1.5 Mn)	0.75	395 (57)	539 (78)	9.4
		336 (49)	458 (68)	7.4
	8	392 (57)	455 (66)	2.8
		364 (53)	414 (60)	2.4
	100	246 (36)	288 (42)	5.2
		257 (37)	308 (45)	4.8

while another set was electrolytically polished. The results of the tensile tests are shown in Table 16. It was found that a solution heat treatment in the lead bath gave the highest yield strength as well as a somewhat higher plastic elongation to fracture. However, these trends were found only for Alloy 1.2, and not for Alloy 1.6 (see Table 16). No significant difference in ductility was found between specimens with and without electropolished surfaces.

Tensile test results for Alloy 1.2 and 1.6, aged at the lower temperature of 453 K (356° F) are shown in Table 17. It was hoped to obtain a higher yield strength in Alloy 1.2 by lowering the aging temperature, which should increase the volume fraction of δ'- and θ'-precipitates. Alloy 1.6 did not show an improvement in the underaged and peak-aged condition, but gave a considerably higher yield strength in the overaged condition (compare Tables 15 and 17). The yield strength of Alloy 1.2 increased slightly in the underaged condition, but showed a more remarkable improvement in the peak and overaged conditions. The large scatter in plastic elongation to fracture values in Table 17 cannot be explained at the moment. It might be due to misalignment of some of the specimens during tensile testing.

TABLE 16. TENSILE PROPERTIES OF ALLOYS 1.2 AND 1.6 IN PEAK-AGED CONDITION (8 h, 473 K) FOR DIFFERENT SHT-PROCEDURES AND SPECIMEN SURFACE CONDITIONS

Alloy No.	SHT in:	$\sigma_{0.2}$ MPa (ksi)	σ_f MPa (ksi)	ϵ_f (%)	Surface Condition*
1.2 (Al-3Li-2Cu-0.2Zr)	Air	400 (58)	487 (71)	2.9	m
	Vacuum	407 (59)	508 (74)	4.3	m
	Lead Bath	425 (62)	553 (80)	4.6	m
	Air	397 (58)	497 (72)	3.8	e
	Vacuum	442 (64)	531 (77)	3.6	e
	Lead Bath	449 (65)	566 (82)	4.9	e
1.6 (Al-3Li-1.5Mn)	Air	436 (63)	509 (74)	2.5	m
	Vacuum	391 (57)	476 (69)	3.0	m
	Lead Bath	429 (62)	499 (72)	2.0	m

*m: mechanically polished (1-μm diamond paste)
e: electrolytically polished

TABLE 17. TENSILE PROPERTIES OF ALLOYS 1.2 (Al-3Li-2Cu-0.2Zr) AND 1.6 (Al-3Li-1.5Mn) FOR VARIOUS AGING TIMES AT 453 K (356° F)

Alloy No.	Aging Time at 453 K (h)	$\sigma_{0.2}$ MPa (ksi)	σ_f MPa (ksi)	ϵ_f (%)
1.2	1	467 (68)	472 (68)	0.5
		387 (56)	387 (56)	0.2
	10	477 (69)	564 (82)	3.6
		468 (68)	566 (82)	3.6
	100	404 (59)	483 (70)	0.5
		412 (60)	427 (62)	0.5
1.6	1	374 (54)	490 (71)	4.7
		380 (55)	509 (74)	5.5
	10	387* (56)	387 (56)	0.1
		368* (53)	375 (54)	0.2
	100	385* (56)	385 (56)	0.1
		370* (54)	370 (54)	0.1

*$\sigma_{0.1}$ – values

TEM examination of foils from deformed tensile samples has been initiated. Preliminary results do not show extensive shear band formations. The observed dislocation distribution seems to be rather uniform, as shown in Fig. 23, and suggests a homogeneous slip distribution. The straight lines on this micrograph are traces of θ' -precipitates and not shear bands.

2.3.3 Fracture Surface Observations

From SEM studies of the fracture surfaces, it was hoped to obtain information about potential crack-nucleation sites and crack-propagation modes. However, the indications are that crack nucleation occurs at the specimen surface. Frequently, long cracks are found on the specimen surfaces, running parallel to the loading axis or extrusion direction (Fig. 24), which might be due to delamination along the flake boundaries. Similar cracks can also be seen on the fracture surfaces, an example of which is shown in Fig. 25.

If one considers the observed fracture topography as the result of crack propagation, then some rather speculative conclusions may be drawn by taking the TEM observations into account. Potential crack propagation modes in both alloys in the under- and peak-aged conditions could be cracking within the PFZs. Also, in Alloy 1.6 a transgranular fracture mode by microvoid nucleation and coalescence at the Mn-rich particles seems to be feasible. In Alloy 1.2, there are the θ'-precipitates which could promote a transgranular dimple type of failure mode, especially in the peak-aged condition where a higher volume fraction of larger θ'-precipitates is observed. The fracture surface features of specimens in the under- and peak-aged conditions suggest the microscopic ductile fracture mode for both alloys is along grain or subgrain boundaries (Figs. 26 through 29). At higher magnifications, the fracture surfaces reveal features with dimensions which are approximately of the same size as the grain or subgrain sizes. (Compare Figs. 26 through 29 with Figs. 8 and 13.) However, more work is required to establish a sound basis for this model.

The fracture surfaces of tensile specimens in the overaged condition of both alloys are different from those of the under- and peak-aged microstructures. The fracture

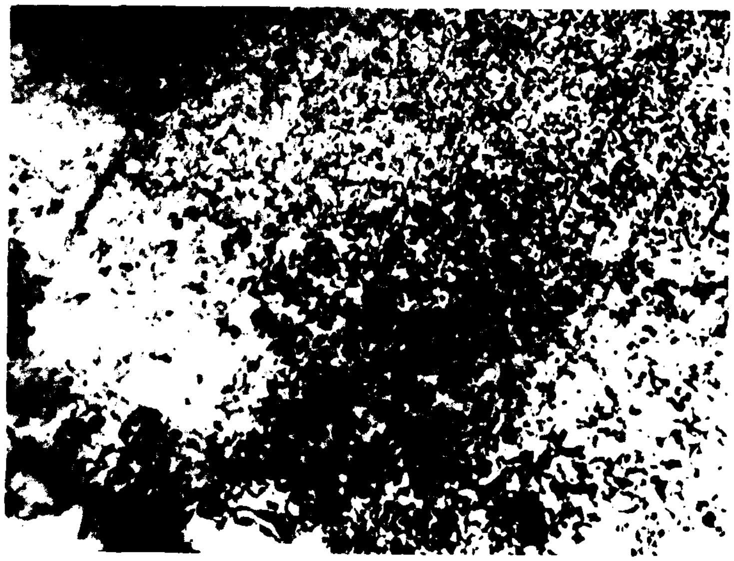

0.2 μm

Figure 23. Deformation structure in fractured tensile specimen of Alloy 1.2 (Al-3Li-2Cu-0.2Zr) (8 h, 473 K) (TEM).

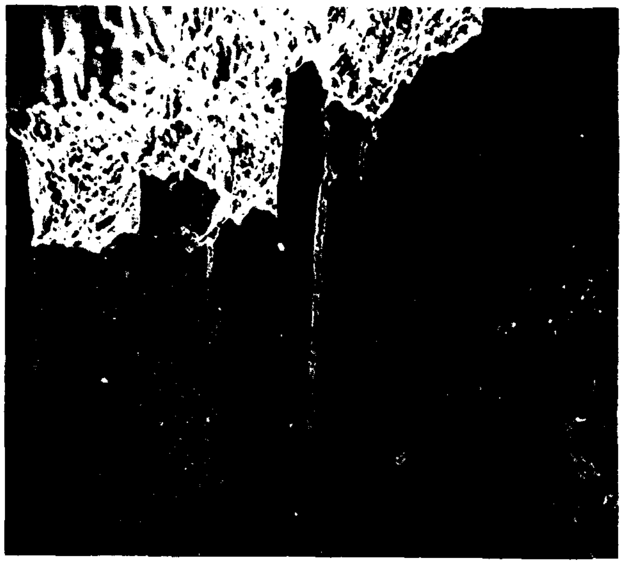

100 μm

Figure 24. Cracks on the surface of a fractured tensile specimen of Alloy 1.2 (Al-3Li-2Cu-0.2Zr), in underaged condition (0.75 h, 473 K) (SEM).

100 μm

Figure 25. Secondary cracking on the fracture surface of Alloy 1.2 (Al-3Li-2Cu-0.2Zr) in underaged condition (0.75 h, 473 K) (SEM).

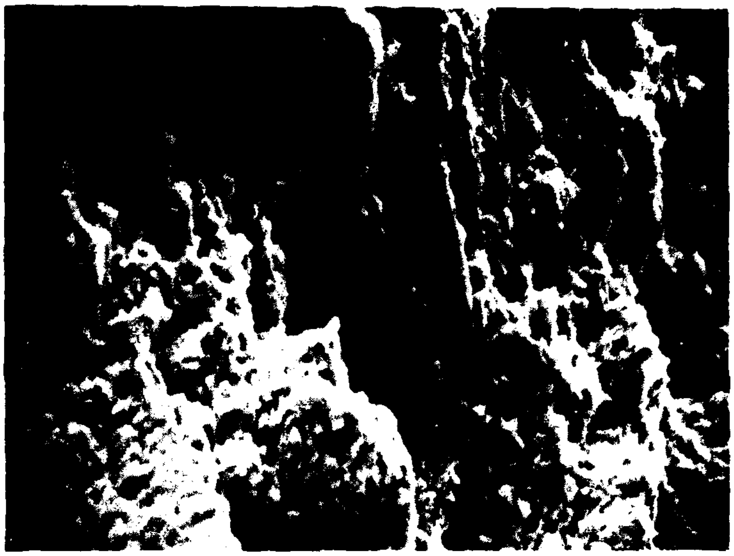

a

40 μm

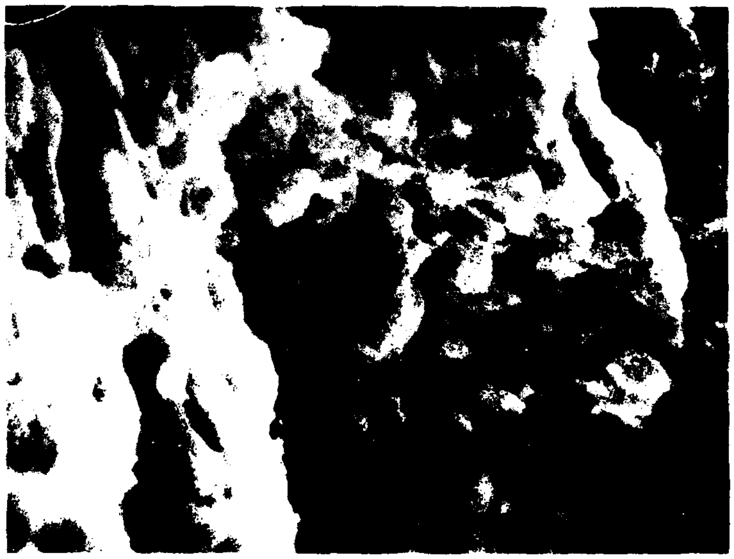

b

10 μm

Figure 26. Fracture surface appearance of tensile specimen, Alloy 1.2 (Al-3Li-2Cu-0.2Zr), in underaged condition (0.75 h, 473 K) (SEM).

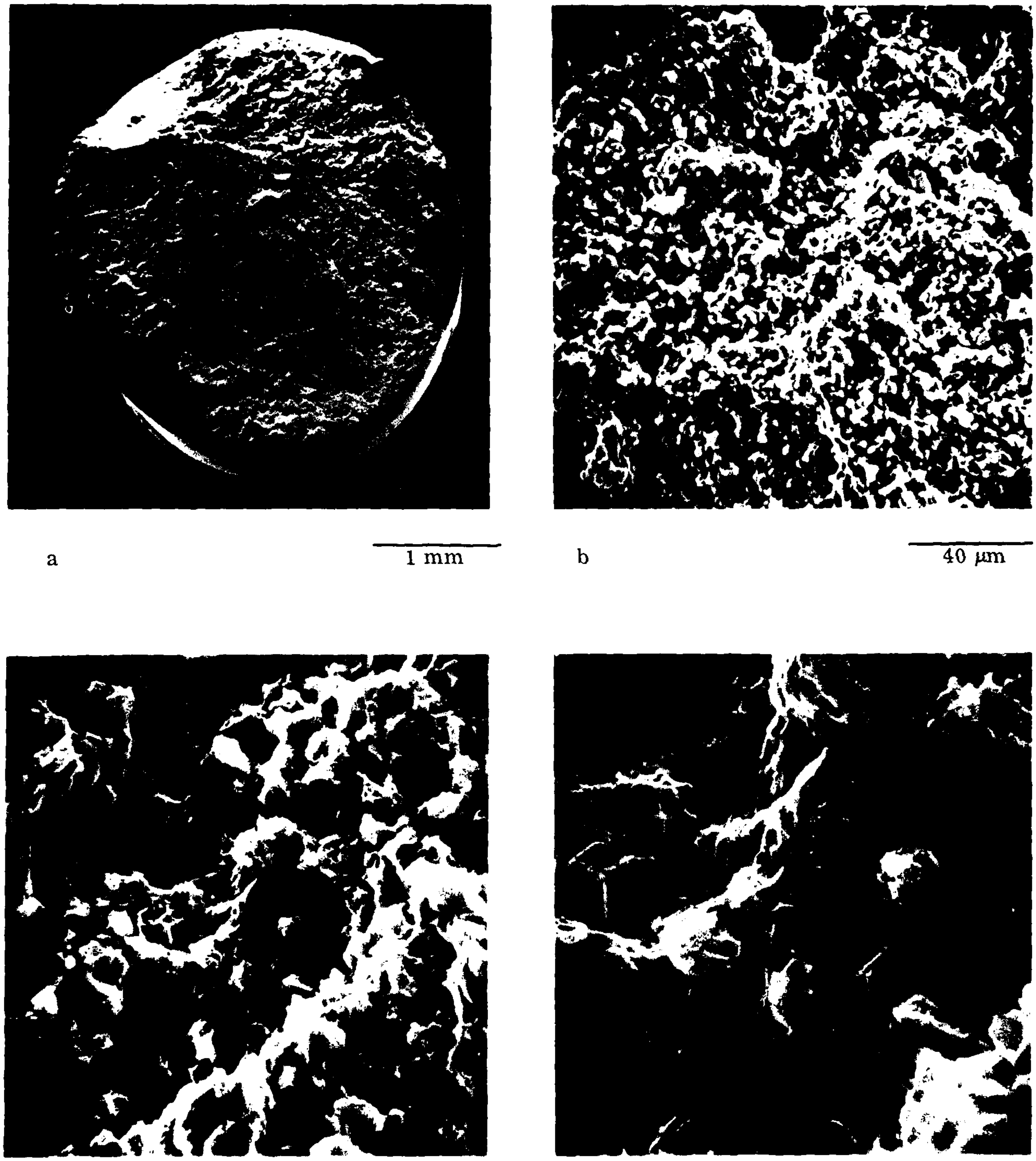

a 1 mm b 40 μm

c 10 μm d 4 μm

Figure 27. Fracture surface appearance of tensile specimen, Alloy 1.2 (Al-3Li-2Cu-0.2Zr) in peak-aged condition (8 h, 473 K) (SEM).

a 1 mm

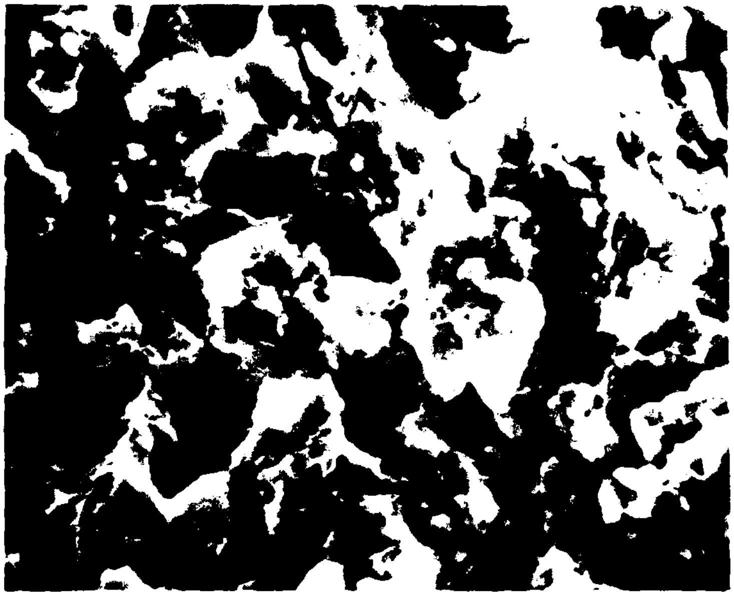

b 10 μm

Figure 28. Fracture surface appearance of tensile specimen, Alloy 1.6 (Al-3Li-1.5Mn), in underaged condition (0.75 h, 473 K) (SEM).

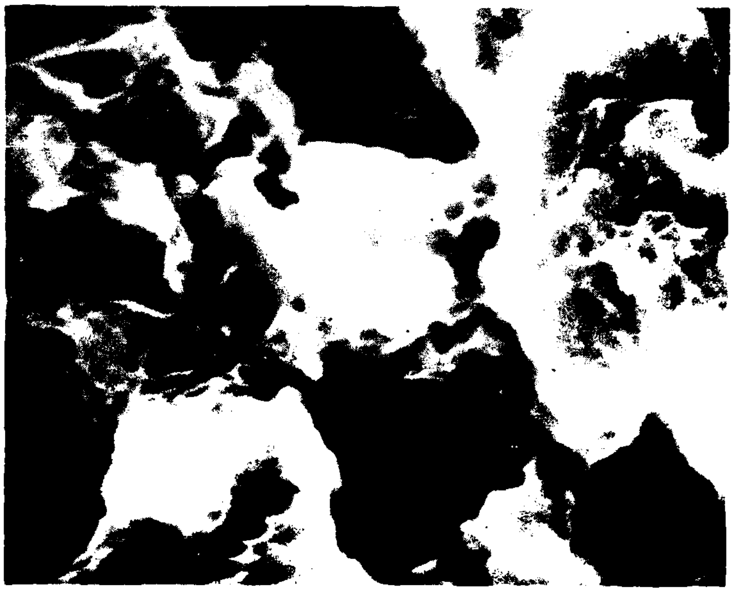

c 4 μm

Figure 28. (Contd.)

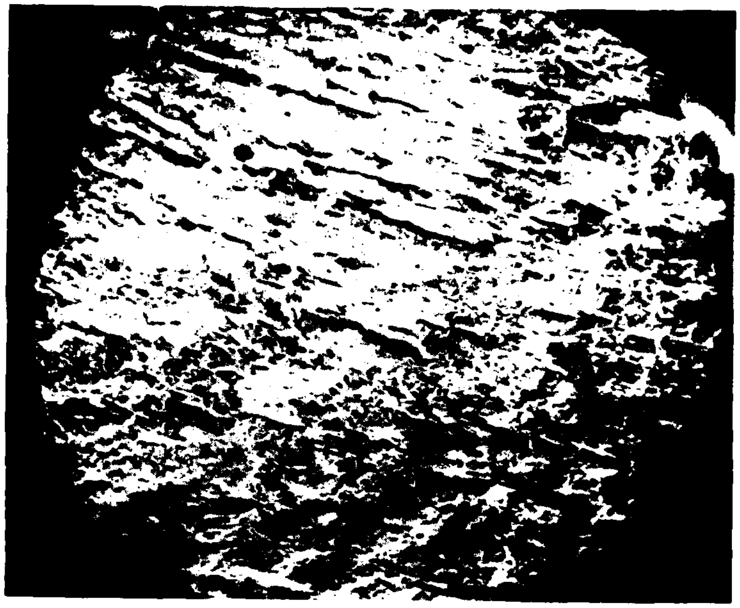

a

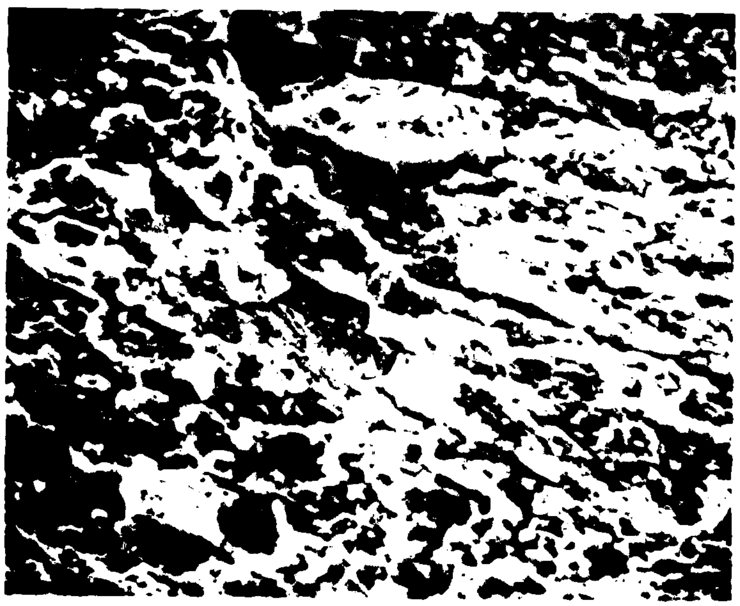

b

Figure 29. Fracture surface appearance of tensile specimen, Alloy 1.6 (Al-3Li-1.5Mn), in peak-aged condition (8 h, 473 K) (SEM).

surfaces, as well as the specimen surfaces, were covered with a reactive surface layer which formed shortly after completion of the tensile tests. This layer is seen on the fracture surface in Figs. 30a and b and on a polished specimen gage section in Fig. 31. It is therefore difficult to decide which of the observed features belong to the fracture process at all. As described above, an effect of surface layer formation occurred on polished samples prepared for light microscopy studies and on TEM foils after storing them in air for a short time, and is more pronounced in Alloy 1.6 than for 1.2.

2.4 TASK 4 — APPLICATION STUDIES

This task is being performed by the Lockheed-California Company.

During this period, there was no work performed on Task 4.

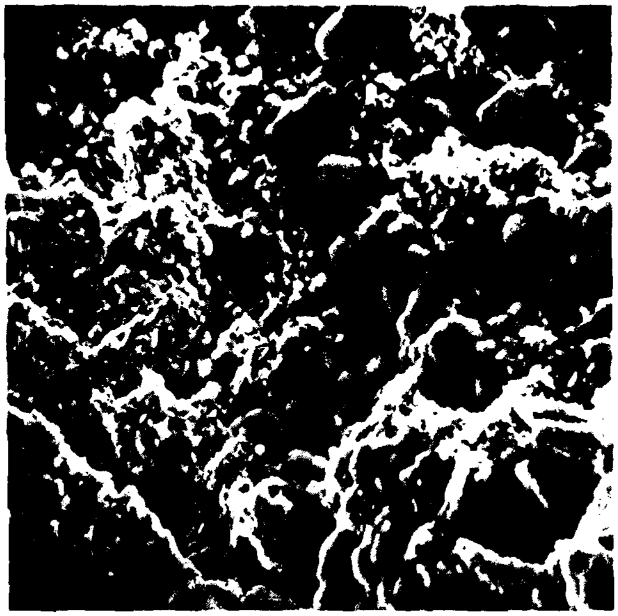

a

40 μm

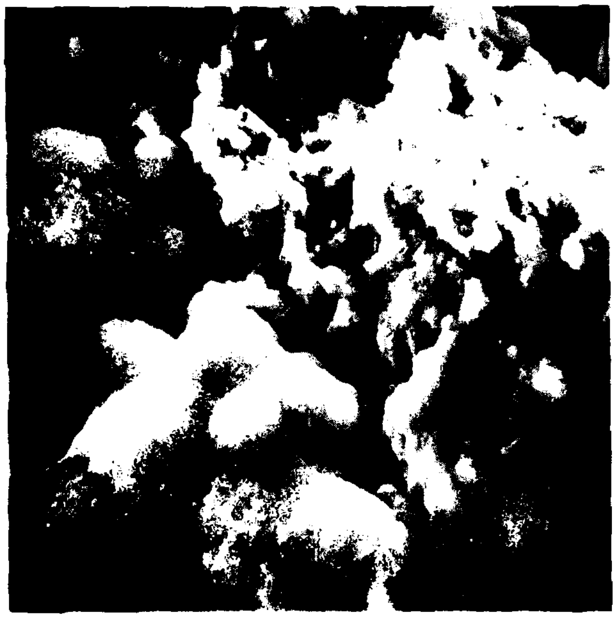

b

10 μm

Figure 30. Fracture surface appearance of tensile specimen, Alloy 1.2 (Al-3Li-2Cu-0.2Zr), in overaged condition (100 h, 473 K): some reaction product covers the surface (SEM).

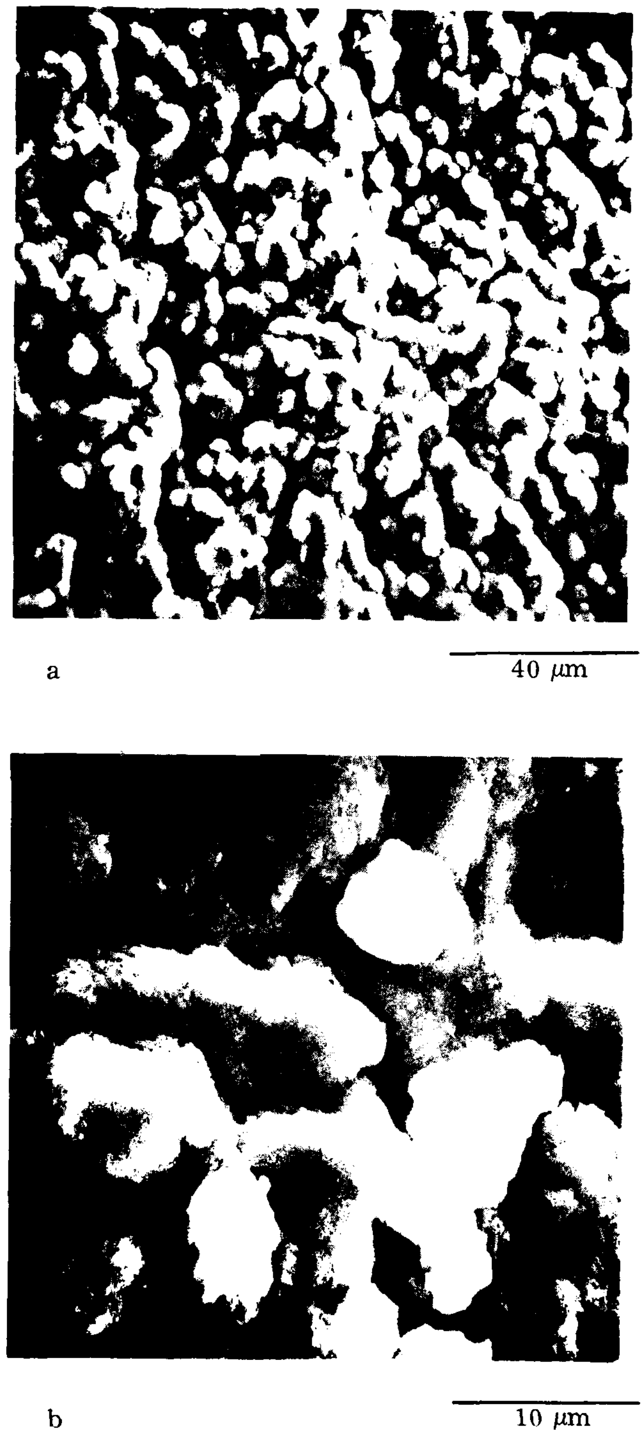

Figure 31. Tensile specimen free surface within polished gage section after testing and storage in air, Alloy 1.2 (Al-3Li-2Cu-0.2Zr) in overaged condition. (Note reaction product covering surface.) (SEM).

Section 3
CONCLUSIONS

1. In the Al-3Li-X alloy splats, tensile strength and elongation values for solution treated and under-, peak-, or overaged conditions of extrusions (8:1 ER), made from screened (-8/+100) splat particulate were similar to identical extrusions made from unscreened particulate. Significant amounts of delamination were observed on the fracture surfaces, with delamination apparently corresponding to prior particle boundaries.

2. Increasing the extrusion ratio from 8:1 to 20:1 for the Al-3Li-X alloys did not significantly change the tensile properties in the solution treated and under-, peak-, or overaged conditions. However, reducing the overaging time from 100 to 40 h at 473K (392° F) for Alloy 1.2A (Al-3Li-2Cu-0.2Zr) produced the best combination of tensile strength and ductility to date: 413 MPa (60 ksi) yield strength and 6.3% elongation. The higher extrusion ratio did, however, reduce the amount of delamination observed on the fracture surfaces. Inclusions possibly associated with nonsplat particles were often found at the fracture origin region of the tensile specimens, suggesting that simple screening does not remove enough of the nonsplat particles to significantly improve the tensile properties.

3. Reducing the Cu content from 4.0 to 2.0 wt.% in Al-3Li splat alloys reduced but did not eliminate the presence of brittle intermetallics of Al-Li-Cu. Elimination of this brittle phase in an Al-3Li-Cu alloy is expected to be achieved by reducing Cu to 1.5 wt.%.

4. Comparison of tensile strength and ductility data for Al-3Li-X alloys in the present study with published results of other studies does not allow the direct evaluation of the effect of alloy composition because of large differences in cross-sectional shape of the various extrusions, and associated (unquantified) differences in crystal texture. Strong differences in crystal texture are known to have a significant effect

on tensile properties of high-strength commercial aluminum alloys.

5. Examination by TEM of thin foils from deformed tensile samples of the Al-3Li-X splat alloys suggests that slip occurs homogeneously. Preliminary results do not show any extensive shear band formation, as reported for ingot metallurgy alloys of comparable composition.

6. At high magnification, tensile fracture surface features in the Al-3Li-X alloys in the under- and peak-aged conditions have about the same dimensions as the subgrain and grain sizes. Further work is required to determine the significance of this observation with respect to identification of microstructural feature(s) dominating the fracture behavior in the Al-3Li-X splat alloys.

7. Thirty five alloy-particulate type-consolidation process combinations of nonlithium-containing alloys designed to produce a high specific stiffness were successfully produced. Alloys included Al-Fe-Ni-Co, Al-Mn, and Al-Mn-Si compositions having either 5 or 7.5 atomic percent solute content. Particulate types included splat produced in air or argon and fine atomized powder produced in air. Because these alloys are nonheat-treatable, vacuum hot pressing and extrusion were conducted at relatively low (various) temperatures. The highest yield strength is exhibited by Alloy 2.4A [Al-4.3 Fe-5Ni-5Co (wt.%)]: 512 MPa (74 ksi), with 3% elongation, and 0.6 NTS/YS ratio. Alloy 2.2A [Al-3.5Fe-2.5Ni-4.2Co (wt.%)] exhibited the best combination of properties: 360 MPa (52 ksi) yield strength, 9% elongation, and 1.5 NTS/YS ratio. Alloy 2.6A [Al-9.7Mn-2.5Si (wt.%)] had the next best combination of properties: 312 MPa (45 ksi) yield strength, 14% elongation, and 1.6 NTS/YS ratio.

8. The addition of 2.5 wt.% Si to an Al-9.7 wt.% Mn alloy increased both tensile ductility and strength, with the possibility that a yield strength increase above 390 MPa (45 ksi) may be achieved with good ductility by addition of more than 2.5 wt.% Si.

9. The tensile properties of Al-Fe-Ni-Co and Al-Mn-Si alloys made from splat particulate were unaffected by splat atmosphere being either air or argon. Tensile properties of the same alloys were similar for both splat and fine atomized powder product, with the latter exhibiting slightly higher strength and lower ductility. The anisotropy of tensile properties (longitudinal versus transverse) was comparable for splat and fine atomized powder products.

Section 4
REFERENCES

1. R. E. Lewis, D. Webster, and I. G. Palmer, A Feasibility Study for Development of Structural Aluminum Alloys From Rapidly Solidified Powders for Aerospace Structural Applications, Lockheed Palo Alto Research Laboratory Final Report, Air Force Contract F33615-77-C-5186, Technical Report No. AFML-TR-78-102, July 1978

2. R. E. Lewis, Development of Advanced Aluminum Alloys from Rapidly Solidified Powders for Aerospace Structural Applications, Interim Technical Report for Period September 1978 – March 1979, Air Force Contract F33615-78-C-5203, ARPA Order No. 3417, March 1979

3. R. E. Lewis, Development of Advanced Aluminum Alloys from Rapidly Solidified Powders for Aerospace Structural Applications, Interim Technical Report for Period March 1979 – September 1979, Air Force Contract F33615-78-C-5203, ARPA Order No. 3417, September 1979

4. T. H. Sanders, Development of an Al-Mg-Li Alloy, Naval Air Development Center Contract No. N62269-74-C-0438, Final Report, June 1976

5. E. J. Coyne, The Effect of Microstructure on the Fatigue Behavior of an Aluminum-Lithium Alloy, Ph.D. Thesis, Georgia Institute of Technology, October 1979

6. T. H. Sanders, Factors Influencing Fracture Toughness and Other Properties of Aluminum-Lithium Alloys, Naval Air Development Center Contract No. N62269-76-C-0271, Final Report, June 1979

7. K. K. Sankaran, Structure and Properties of Splat Quenched 2024-Type Aluminum Alloys Containing Lithium, Ph.D. Thesis, Massachussetts Institute of Technology, Cambridge, 1978

8. D. Webster, "Properties and Microstructure of Aluminum-Copper-Magnesium-Lithium Alloys," Met. Trans. A., Vol. 10A, 1979, p. 1913

9. Fulmer Research Institute, "Low Density, High Strength Al-Mg Alloys Containing Lithium," undated advertising flyer

10. W. S. Cebulak and D. J. Truax, Program to Develop High Strength Aluminum Powder Metallurgy Products, Phase III—Scale Up A, Contract DAAA25-70-C0358, Final Report, Sept. 29, 1972

11. R. E. Sanders, G. J. Hildeman, and D. J. Lege, Elevated Temperature Alloy Development, Alcoa Annual Technical Report on Air Force Contract F33615-77-C-5086, March 1979